NATIONAL ADVISORY COMMITTEE FOR AERONAUTICS

TECHNICAL NOTE 2598

A TECHNIQUE APPLICABLE TO THE AERODYNAMIC DESIGN OF INDUCER-TYPE MULTISTAGE AXIAL-FLOW COMPRESSORS

By Melvyn Savage and Loren A. Beatty

Langley Aeronautical Laboratory
Langley Field, Va.

Washington
March 1952

ERRATA NO. 1

NACA TN 2598

A TECHNIQUE APPLICABLE TO THE AERODYNAMIC DESIGN OF INDUCER-TYPE MULTISTAGE AXIAL-FLOW COMPRESSORS

By Melvyn Savage and Loren A. Beatty

March 1952

In order to correct any misconceptions concerning the exact nature of the basic equations of this paper, the paragraph beginning on line 4 of page 9 should be replaced by the following paragraph:

"For an untapered passage, adding the same radially constant power input in each of the remaining stages as was applied in the second stage would maintain the prescribed constant inlet-axial-velocity distribution for these stages. For a tapered passage, the required radial total-temperature gradient decreases with increasing hub-tip ratio. It was assumed, for preliminary design studies, that constant rotor-inlet axial velocity could be maintained for all stages after the first by adding a radially constant power input in these stages. It was also assumed that the magnitude of this power input could be varied from stage to stage within the loading limits for each stage. These assumptions are sufficiently accurate for preliminary design studies such as those presented in this paper. For a detailed design, however, it may be desirable to consider the small radial variation in rotor-inlet axial velocity which occurs when the variation in required total-temperature gradient associated with varying hub-tip ratio is ignored and when the magnitude of the stage power input is varied from stage to stage."

TABLE OF CONTENTS

NATIONAL ADVISORY COMMITTEE FOR AERONAUTICS

TECHNICAL NOTE 2598

A TECHNIQUE APPLICABLE TO THE AERODYNAMIC DESIGN OF INDUCER-TYPE MULTISTAGE AXIAL-FLOW COMPRESSORS

By Melvyn Savage and Loren A. Beatty

SUMMARY

A method is presented for the preliminary design calculation of high-pressure-ratio, multistage, axial-flow compressors using the solid-body inducer-type design. Compressors of this type of design have an inducer first stage which sets up a prescribed total-temperature distribution so that the inlet axial velocity to the second stage is radially constant. The remaining stages have radially constant power input, average tangential velocity proportional to the radius, and radially constant rotor inlet axial velocities equal to the inlet axial velocity of the compressor. A chart which facilitates preliminary design calculations for any solid-body inducer-type design is presented.

Typical preliminary design calculations are presented for inlet hub-tip ratios of 0.40, 0.50, and 0.60 with weight flows ranging from 20.0 to 32.5 pounds per second per square foot of frontal area and average pressure ratios per stage ranging from 1.28 to 1.38. From these calculations some of the effects of specific weight flow, rotational speed, hub-tip ratio, turning angle, and inlet air angle on power input, amount of radial flow, and over-all pressure ratio are investigated.

INTRODUCTION

Cycle analyses of aircraft propulsion systems indicate that a better balance among weight, thrust, and specific fuel consumption can often be obtained through utilization of over-all compressor pressure ratios higher than those now used in current practice (references 1 and 2). Hence, the design of efficient high-pressure-ratio compressors appears to be important.

It is felt that average pressure ratios per stage can be greater than present-day values with negligible change in compressor efficiency. Greater stage pressure ratios would either reduce the compressor length, weight, and cost or, within these limitations of the same length, weight, and cost, permit the design of compressors having higher over-all pressure ratios.

Since two-dimensional free-vortex multistage designs cannot yield high average stage pressure ratios or high weight flows, various other types of stage design have been investigated (for example, see reference 3). Generally, these other types have radial flows entailing three-dimensional-flow calculations. A procedure for calculating the characteristics of a compressor of any given type of design taking into account the effect of radial motion of the gas is presented in reference 4.

Solid-body rotor tests, for example, reference 3, indicate that three-dimensional flows may be utilized with high efficiency. Tests reported in reference 5 on a solid-body and a free-vortex stage indicated that the solid-body stage had as high an efficiency as the more conventional free-vortex stage. In both references it was determined that the three-dimensional theory used in conjunction with two-dimensional cascade data is sufficiently accurate for design purposes.

An analysis of the characteristics of multistage compressors, composed of solid-body stages having constant power input and approximately symmetrical velocity diagrams at all radii, was presented in reference 6. Average stage pressure ratios for the designs calculated ranged from 1.25 to 1.35. The maximum Mach numbers for this type of design occur at the stator inlet, hub end. The rotational speed and hence the amount of pressure rise possible are limited by the fact that the axial velocities occurring at the stator inlet, hub end, are large. In the type of design to be investigated in this paper, these axial velocities are much lower than those of reference 6 and therefore permit higher rotational speeds and hence higher pressure ratios for the same critical Mach number limitation. This axial-velocity effect is most noticeable at the lower hub-tip ratios which occur in the early stages of a compressor.

The type of design for solid-body multistage compressors being investigated herein differs from that in reference 6 in that the first stage has the radial power-input distribution required to make the inlet axial velocity to the second stage constant radially rather than a radially constant power input. This first stage will be termed the inducer stage. The stages succeeding the inducer stage have:

(1) Constant power input from hub to tip

(2) Radially constant rotor inlet axial velocity

(3) A variable hub radius to maintain a constant mean axial velocity through the compressor

(4) Approximately symmetrical velocity diagrams in the tangential direction from hub to tip

(5) A turning angle and Mach number limitation based on cascade data

This type of design is termed an inducer compressor design.

Simplified, general, three-dimensional compressible-flow equations are derived which permit the calculation of the axial-velocity distribution at any station between blade rows. These equations are then applied to the inducer compressor design described previously. A design method for this type of multistage compressor is presented which satisfies continuity directly and permits a rapid calculation of the velocity diagrams for all the stages. Calculations of several multistage compressor designs are made at inlet hub-tip ratios of 0.40, 0.50, and 0.60 over the practical range of design weight flows.

This investigation, conducted at the Langley Aeronautical Laboratory of the National Advisory Committee for Aeronautics, was completed in June 1950.

SYMBOLS

A	annulus area
A_f	frontal area
a	sonic velocity
c_p	specific heat of gas at constant pressure
c_v	specific heat of gas at constant volume
n	polytropic exponent of compression
n'	polytropic exponent of expansion
p	static pressure
P	total pressure
r	radius measured from axis of compressor
s	entropy

t	static temperature
T	total temperature
V_u	absolute tangential velocity component
$V_{u_{av}}$	average absolute tangential velocity component obtained by averaging the blade-row inlet and exit absolute tangential velocity components
U	rotational speed $(r\omega)$
V	absolute velocity
W	velocity relative to rotor blade
ΔW_u	change in tangential velocity across a rotor
w	weight flow
β	angle between relative inlet air velocity and compressor axis
γ	ratio of specific heats $\left(c_p/c_v\right)$
η	efficiency
θ	turning angle
ρ	density
σ	blade solidity (Chord/Gap)
ω	angular velocity
$\frac{U\,\Delta W_u}{V_{a_1}^2}$	power-input ratio
$\frac{V_a}{V_{a_1}}$	axial-velocity ratio
$\frac{V_u}{V_{a_1}}$	absolute-tangential-velocity ratio

$\frac{U}{V_{a_1}}$ rotational-speed ratio

$\frac{r_h}{r_t}$ hub-tip radio

Subscripts:

1, 2, 3, 4, . . . stations (see fig. 1)

GV guide vane

a axial direction

h hub section

i inlet station

e exit station

k stations 2, 4, 6, . . .

m mean-radius section

n stage number

s stator coordinates

t tip section

x,y radial positions

A symmetrical stage is herein defined as one in which $U = V_{u_i} + V_{u_e}$.

ANALYSIS

In the conventional type of free-vortex stage the axial velocity remains constant across the blade row. This flow condition is two-dimensional in that the streamlines lie on circular cylinders and do not shift radially. In order to get pressure ratios of approximately 1.3 and high weight flows per square foot of frontal area, the blade loading associated with the free-vortex type of design has to be abandoned. Any variation from this blade loading usually means that the flow will be three-dimensional in that a radial variation in axial velocity between blade rows results (reference 7).

Basic Equations

In order to determine the three-dimensional-flow equations, the assumption is made that simplified radial equilibrium exists between blade rows, that is, the effect of streamline curvature caused by radial flows is neglected. According to tests conducted in reference 8 simplified radial equilibrium was quickly established at about 1/3 chord downstream from the blade row. The radial-equilibrium equation therefore becomes $\frac{dp}{dr} = \rho \frac{V_u^2}{r}$. It is also assumed that the flow is compressible. The coordinate system and some of the symbols used in this paper are indicated in figures 1 and 2.

A detailed derivation of both general and specific equations is given in appendix A. An expression for the differences between axial velocities leaving the rotor at any two radial positions as a function of the conditions ahead of the rotor, the power-input distribution, and the tangential-velocity distribution behind the rotor is derived in appendix A and is as follows:

$$V_{a_e}^2 - V_{a_{e_m}}^2 = \left(2U\,\Delta W_u + V_{a_i}^2 + V_{u_i}^2 - V_{u_e}^2\right) - \left(2U_m\,\Delta W_{u_m} + V_{a_{i_m}}^2 + V_{u_{i_m}}^2 - V_{u_{e_m}}^2\right) + 2\int_{r_m}^{r} \frac{V_{u_i}^2}{r}\,dr - 2\int_{r_m}^{r} \frac{V_{u_e}^2}{r}\,dr \qquad (1)$$

where the radial gradient of entropy is zero at both inlet and exit stations. Equation (1) is the same as that derived for incompressible flow in reference 3. The equation is general since the distributions of power input, tangential velocity, and inlet axial velocity are not specifically defined.

For the axial-velocity differences behind a stator, the power-input terms drop out of equation (1) and it becomes:

$$V_{a_e}^2 - V_{a_{e_m}}^2 = \left(V_{a_i}^2 + V_{u_i}^2 - V_{u_e}^2\right) - \left(V_{a_{i_m}}^2 + V_{u_{i_m}}^2 - V_{u_{e_m}}^2\right) + 2\int_{r_m}^{r} \frac{V_{u_i}^2}{r}\,dr - 2\int_{r_m}^{r} \frac{V_{u_e}^2}{r}\,dr \qquad (2)$$

This stator equation is quite general in that no particular condition ahead of the stator and no particular type of tangential-velocity distribution have been been specified.

For the axial-velocity differences behind a guide vane, the inlet axial velocity is constant and there are no entering tangential velocity components; hence, equation (2) becomes:

$$V_{a_e}^2 - V_{a_{e_m}}^2 = V_{u_{e_m}}^2 - V_{u_e}^2 - 2\int_{r_m}^{r} \frac{V_{u_e}^2}{r}\,dr \qquad (3)$$

This equation is general in that the tangential-velocity distribution leaving the guide vane is not specified.

In using any of the equations to determine the actual values of axial velocity, the continuity equation must be satisfied. When power input, weight flow, total temperature, hub-tip ratio, and rotational speed are known, continuity may be satisfied by one of the following methods:

Method A (exact method): A value of axial velocity at some radial station such as the mean radius is selected. Then, by using the appropriate equation ((1), (2), or (3)) the axial velocities are determined so that the corresponding density values can be calculated. The chosen value of mean-radius axial velocity is then varied until the weight flow obtained by integrating the plot of ρV_a against r^2 coincides with the design weight flow.

Method B (simplified method): Method A can be simplified when the following conditions are met:

(1) The radial distribution of density is linear and therefore the mean radius density and the radial-average density are coincident

(2) The quantity of flow in the part of the annulus above the mean radius equals that below it

(3) The magnitude of the area contraction is that required to counterbalance the effect of the increase in average density across the blade rows and hence maintain a constant average axial velocity

When the preceding conditions are met, continuity may be satisfied by plotting V_{a_e}/V_{a_1} against r^2 and altering the choice of the

mean-radius axial velocity until the plotted area above $\frac{V_{a_i}}{V_{a_1}} = 1.00$ exactly equals that below it.

The type of inducer compressor design investigated in this paper rather closely satisfied the previously mentioned conditions under which method B is applicable. Values of axial velocities calculated by using method B were found to be practically the same as those obtained by using method A. Hence method B was used for the design calculation presented.

Solid-Body Inducer Design

A compressor composed of solid-body stages designed with $V_{u_{av}}$ proportional to radius and with constant power input from hub to tip would permit high stage pressure ratios at high weight flows without exceeding the Mach number and turning-angle limitations. For a non-tapered passage these stage design conditions would result in symmetrical velocity diagrams at all radial positions. This type of axial-flow compressor was investigated in reference 6.

By use of an inducer first stage, a radially constant second-stage V_a distribution may be specified at either the rotor inlet or exit. Another possibility is to specify that the average axial velocity across the rotor is radially constant. For all such designs the Mach numbers are reduced at the hub sections where the maximum Mach numbers occur for the design of reference 6 which is not an inducer type. Each such prescribed constant V_a distribution would require a specific total-temperature distribution which can be produced by a suitable inducer-stage radial distribution of power input. Both the radial gradient of power input required in the inducer stage and the critical Mach number difficulties occurring at the tip in the succeeding stages are reduced as the location of the constant V_a distribution is changed from rotor exit, to the average (across the rotor), to the rotor inlet. These trends can be seen by noting that, for zero radial gradient of power input in the first stage, the V_a at the inlet to the second-stage rotor decreases from hub to tip and the V_a at the exit of this rotor also decreases but at a greater rate. Then, for V_a constant at the second-stage rotor inlet, the rate of decrease from hub to tip at the exit is reduced. For a constant V_a at the second-stage rotor exit, the V_a at the second stage rotor inlet must increase from hub to tip. Each change toward a greater increase in V_a from hub to tip at the second-stage rotor inlet requires a greater radial gradient of power input in the inducer stage. Hence it was decided to investigate the

type of design in which all stages after the inducer stage would have radially constant axial velocity at the rotor inlet and thereby allow greater power input in these stages for the same Mach number limitation.

For an untapered passage, adding a radially constant power input in each of the remaining stages would maintain the prescribed axial-velocity distribution for these stages. For a tapered passage, the required radial total-temperature gradient decreases with increasing hub-tip ratio. The assumption that adding a constant power input in the remaining stages would maintain the prescribed axial-velocity distributions for these stages is sufficiently accurate for preliminary designs such as those presented in this paper. For a detailed design, however, it may be desirable to consider this variation in required total-temperature gradient associated with varying hub-tip ratio.

The inducer or first-stage power-input distribution necessary to produce constant rotor inlet axial velocity for the second stage is derived in appendix A. It was found to be

$$U\,\Delta W_u = U_m\,\Delta W_{u_m} + \frac{V_{u_4}^2 - V_{u_{4_m}}^2}{2} + \int_{r_m}^{r} \frac{V_{u_4}^2}{r}\,dr \qquad (4)$$

Equation (4) states that the power input of the inducer stage at any radial position is a function of the tangential-velocity distribution entering the second rotor and a chosen inducer mean-radius power input.

Writing the general rotor equation (equation (1)) for the inducer rotor and substituting the expression given in equation (4) for the power-input distribution results in:

$$V_{a_3}^2 = V_{a_{3_m}}^2 + \left(V_{a_2}^2 + V_{u_2}^2 - V_{u_3}^2\right) - \left(V_{a_{2_m}}^2 + V_{u_{2_m}}^2 - V_{u_{3_m}}^2\right) + V_{u_4}^2 -$$

$$V_{u_{4_m}}^2 + 2\int_{r_m}^{r} \frac{V_{u_2}^2}{r}\,dr - 2\int_{r_m}^{r} \frac{V_{u_3}^2}{r}\,dr + 2\int_{r_m}^{r} \frac{V_{u_4}^2}{r}\,dr \qquad (5)$$

Equation (3) for the guide-vane-exit axial-velocity distribution at station 2 becomes

$$V_{a_2}^2 = V_{a_{2_m}}^2 + V_{u_{2_m}}^2 - V_{u_2}^2 - 2\int_{r_m}^{r} \frac{V_{u_2}^2}{r}\,dr \tag{6}$$

Substituting the expression for $V_{a_2}^2$ given by equation (6) into equation (5) yields the equation

$$V_{a_3}^2 = V_{a_{3_m}}^2 - \left(V_{u_3}^2 - V_{u_{3_m}}^2\right) + V_{u_4}^2 - V_{u_{4_m}}^2 - 2\int_{r_m}^{r} \frac{V_{u_3}^2}{r}\,dr + 2\int_{r_m}^{r} \frac{V_{u_4}^2}{r}\,dr \tag{7}$$

This equation states that the axial-velocity distribution leaving the inducer-stage rotor is a function of the inducer-stage rotor-exit tangential-velocity distribution and the tangential-velocity distribution entering the second-stage rotor. The second-stage inlet tangential velocities must be known in order to solve this equation. Hence it is necessary to design the second stage before designing the inducer stage.

The equation for the axial-velocity distribution at the exit of the succeeding rotors, which have constant power-input distributions, constant inlet axial velocities, and average tangential velocity proportional to the radius, is derived in appendix A as

$$V_{a_e}^2 = V_{a_{e_m}}^2 - 2U\,\Delta W_u \log_e \frac{r}{r_m} \tag{8}$$

METHOD OF CALCULATION OF MULTISTAGE INDUCER COMPRESSOR DESIGN

Design Chart for Simplifying Calculations

The design calculation for any combination of weight flow and rotational speed can be simplified by the preparation of a chart presenting

the relations between the design variables in the range applicable to the design under consideration.

Basic chart.- The basic chart is prepared as follows: Dividing equation (8) by $V_{a_1}^2$ to make it dimensionless results in

$$\left(\frac{V_{a_e}}{V_{a_1}}\right)^2 = \left(\frac{V_{a_{e_m}}}{V_{a_1}}\right)^2 - 2\,\frac{U\,\Delta W_u}{V_{a_1}^2}\log_e\frac{r}{r_m} \tag{9}$$

This equation combined with method B for satisfying continuity will give the actual values of axial-velocity ratio for each combination of power-input ratio $U\,\Delta W_u/V_{a_1}^2$ and hub-tip ratio r_h/r_t.

This type of calculation was completed for hub-tip ratios ranging from 0.40 to 0.95 in increments of 0.05 and for a range of power-input ratios covering the region of interest for practically all stage designs. Figure 3 is a plot of these calculations and shows the power-input ratio plotted against hub axial-velocity ratio for various hub-tip ratios. This plot is general in that no particular rotational speed, inlet axial velocity, or inlet total temperature has been specified; however, it applies only to those stages in the solid-body inducer compressor design that succeed the inducer stage.

Curves of constant hub turning angle.- Curves of constant hub turning angle may be drawn in figure 3 for any particular rotational-speed ratio, U/V_{a_1}. These curves aid greatly in choosing the maximum power input for a stage when turning angle is the limiting factor. The method of drawing curves of constant hub turning angle is as follows:

(1) The hub turning angle θ_h is defined as

$$\tan^{-1}\frac{(V_{u_e})_h}{V_{a_1}} - \tan^{-1}\frac{(V_{u_i})_h}{(V_{a_e})_h}$$

(2) A value of θ_h is selected

(3) When a power input and hub-tip ratio are chosen, $(V_{a_e})_h$ can be calculated from the preceding relationship for θ_h

(4) Several choices of power input are usually necessary to make the calculated value of $(V_{a_e})_h$ coincide with the value satisfying continuity determined by using figure 3

(5) This procedure, repeated for several hub-tip ratios, will allow a curve of constant θ_h to be drawn in figure 3

Examples of curves of constant θ_h on the axes of figure 3 will be presented subsequently.

Curves of constant hub inlet air angle.- Curves of constant hub inlet air angle β_h may also be drawn quite easily in figure 3 for any particular rotational-speed ratio U/V_{a_1}. These curves of constant β_h aid greatly in regions where the variation of hub-turning-angle limitation with inlet air angle is important.

Figure 4 is a plot of power-input ratio against rotational-speed ratio U/V_{a_1} for various constant β values. These curves were obtained by using the following relations:

$$\tan \beta = \frac{V_{u_e}}{V_{a_1}}$$

$$\frac{U \Delta W_u}{V_{a_1}^2} = \tan^2\beta - \left(\frac{V_{u_i}}{V_{a_1}}\right)^2$$

$$\frac{V_{u_i}}{V_{a_1}} + \frac{V_{u_e}}{V_{a_1}} = \frac{U}{V_{a_1}}$$

The dashed portions of these curves show the region in which the turning angle is greater than the inlet air angle. Excluding this region, the following trends may be observed:

(1) For constant power-input ratio, β increases as the rotational-speed ratio increases

(2) For constant rotational-speed ratio, β increases as the power-input ratio increases

(3) For constant β, the power-input ratio decreases as the rotational-speed ratio increases

The procedure for drawing curves of constant hub inlet air angle in figure 3 is as follows:

(1) For a chosen U/V_{a_1} determine the values of U_h/V_{a_1} associated with several values of r_h/r_t

(2) With the values of U_h/V_{a_1} and a constant β_h, figure 4 yields the appropriate values of $U\,\Delta W_u/V_{a_1}{}^2$

(3) With the values of $U\,\Delta W_u/V_{a_1}{}^2$ and their respective values of r_h/r_t, the curve of constant hub inlet air angle can be drawn in figure 3

Curves of constant β_h together with the previously described curves of constant θ_h for two values of U_t/V_{a_1} (1.821 and 2.003, which is 10 percent greater than 1.821) are shown in figure 5. This figure is general in that, while U_t/V_{a_1} is specified, no particular rotational speed, inlet axial velocity, or weight flow has been specified. The curves of constant β_h were not continued beyond the point where $\beta_h = \theta_h$.

Special considerations of design chart.- Certain trends caused by alteration of design variables are of importance to the designer. Before examining these trends, it should be noted that a measure of the amount of radial flow in a blade row can be determined by noting the amount of axial-velocity change across the blade row. From an examination of figure 5 the following trends can be obtained:

(1) For constant power-input ratio the radial flow decreases as the hub-tip ratio increases

(2) For constant hub-tip ratio, the radial flow increases as power-input ratio increases

(3) For constant hub turning angle and constant tip-rotational-speed ratio:

  (a) power-input ratio increases as the hub-tip ratio increases

  (b) radial flow decreases as the power-input ratio increases

  (c) radial flow decreases as the hub-tip ratio increases

  (d) hub inlet angle increases as the power-input ratio increases

(4) For constant hub-tip ratio:

(a) hub turning angle increases as the power-input ratio increases for a given tip-rotational-speed ratio.

(b) hub inlet angle increases as the power-input ratio increases for a given tip-rotational-speed ratio

(5) For constant hub turning angles and hub-tip ratio, the power-input ratio, the amount of radial flow, and the hub inlet angle all increased as tip-rotational-speed ratio increased

(6) For a constant V_{a_1} an appreciable increase in power input is possible, within the same hub-turning-angle limitations, for a moderate increase in the tip rotational speed (10 percent in this case). The amount of tip rotational speed possible is limited by the Mach number or turning-angle limitations in the early stages.

Method of Maintaining Constant Average Axial Velocity from Stage to Stage

Each stage calculation is completed by assuming an untapered passage and by using the hub-tip ratio which corresponds to the station between the rotor and stator. If the mean-radius density and mean-radius axial velocity are assumed equal to the radial-average density and radial-average axial velocity at each station, the continuity equation is as follows:

$$A_1\left(\rho_1 V_{a_1}\right)_m = A_k\left(\rho_k V_{a_k}\right)_m \tag{10}$$

where k represents station 2, 4, 6, 8, and so forth. Then at the mean-radius section:

$$\left(\frac{\rho_k}{\rho_1}\right)_m = \left(\frac{\rho_k}{\rho_2}\frac{\rho_2}{\rho_1}\right)_m = \left[\left(\frac{t_k}{t_2}\right)^{\frac{1}{n-1}}\left(\frac{t_2}{t_1}\right)^{\frac{1}{n'-1}}\right]_m \tag{11}$$

where, for the guide-vane expansion process from 1 to 2, $\frac{n' - 1}{n'} = \eta_{GV}\frac{\gamma - 1}{\gamma}$

and, for the compression process, $\frac{n - 1}{n} = \frac{1}{\eta}\frac{\gamma - 1}{\gamma}$.

If the assumption is made that the tip radius is held constant and the annulus contraction rate is such that the radial-average axial velocity remains constant from stage to stage, it follows from equation (10) that:

$$\left(\frac{\rho_k}{\rho_1}\right)_m = \frac{A_1}{A_k} = \frac{1 - \left(\frac{r_h}{r_t}\right)_1^2}{1 - \left(\frac{r_h}{r_t}\right)_k^2} \tag{12}$$

Combining equations (11) and (12) and solving for $\left(\frac{r_h}{r_t}\right)_k^2$ yields

$$\left(\frac{r_h}{r_t}\right)_k^2 = 1 - \frac{1 - \left(\frac{r_h}{r_t}\right)_1^2}{\left[\left(\frac{t_k}{t_2}\right)^{\frac{1}{n-1}} \left(\frac{t_2}{t_1}\right)^{\frac{1}{n'-1}}\right]_m} \tag{13}$$

In order to obtain t_k (the static temperature at a stage exit), the stage exit velocity, that is, the inlet velocity of the succeeding stage, must be determined. As a first approximation, the exit velocity can be assumed equal to the stage inlet velocity. If necessary, this assumption can be modified on completing the design of the succeeding stage.

The velocity diagrams calculated by using the value of r_h/r_t between the rotor and the stator for each stage are symmetrical in the tangential direction in all stages except the inducer stage. Since the actual compressor hub is tapered, very likely, in a detailed design in which the previously mentioned effects of taper are taken into account, some form of correction to the velocity diagrams also should be made. One method of more accurately accounting for taper would be to recalculate the design by assuming a constant hub-tip ratio for each blade row rather than each stage. The constant blade-row hub-tip ratio would be the average of the actual inlet and exit hub-tip ratios of the blade row. If the resulting hub-tip ratios are used in determining the velocity diagrams, the diagrams would no longer be exactly symmetrical in the tangential direction.

Stage Design Procedure

The order of procedure in the design of the solid-body inducer compressor is unusual in that to obtain the axial-velocity distribution leaving the first stage requires that the second-stage tangential-velocity distribution be known and hence the second stage must be designed first. Since it is less difficult to design the stages which succeed the first two, the order of presentation in this paper will be (1) to discuss the design of those stages succeeding the second stage, (2) to discuss the design of the second stage, and (3) to discuss the design of the first stage.

Stages following the second.- The assumption is made that the results obtained in the design of the first and second stages are known. The second-stage hub-tip ratio, denoted by b in figure 6, corresponds to the value of r_h/r_t that occurs at station 5 when equation (13) is used to locate points a and c. For the third-stage calculation, an arbitrary hub-tip ratio e is selected and the design chart, figure 3, is used to choose a power input and to determine the rotor-exit axial velocity at the hub. The velocity diagram and the temperatures are calculated and equation (13) is used to obtain $(r_h/r_t)_8$ which is denoted by f in figure 6. A smooth curve is drawn from a-c to f. The third-stage hub-tip ratio e is altered until it coincides with d which is the value of r_h/r_t that occurs at station 7 according to the curve a-c-f. This procedure is repeated from stage to stage and, after some practice, selection of the correct hub-tip ratios requires only one or two trials.

The amount of power input for each stage is determined by the turning angle and Mach number limitation and how close to these limits the designer wishes to work. For example, a compressor could be designed so that the power input in the later stages (where the loading limitation is caused by turning angle and not Mach number) is that required to maintain constant hub turning angles at or below the limiting turning angle. In this case, a plot such as figure 5, applied to the particular design with the desired turning-angle line, would be considerably helpful. The calculation procedure under these circumstances would be as follows:

(1) Since the rotational-speed ratio is known, a curve of constant hub turning angle is drawn on the design chart by the method previously discussed.

(2) The stages are calculated as already discussed in this section except that the choices of $U\,\Delta W_u/V_{a_1}{}^2$ and r_h/r_t should be made along the prescribed turning-angle curve. The velocities and temperatures at

the hub, mean radius, and tip can easily be computed by using figure 3, equation (9), and the following relationships:

$$\frac{V_{u_i}}{V_{a_1}} = \frac{U - \Delta W_u}{2V_{a_1}}$$

$$\frac{V_{u_e}}{V_{a_1}} = \frac{U + \Delta W_u}{2V_{a_1}}$$

$$c_p \Delta T = U \Delta W_u$$

It is advisable in the early stages to calculate the temperatures and check the absolute Mach number at the stator hub exit and the Mach number relative to the rotor at the rotor tip inlet to insure that the Mach number limitation is not exceeded.

Inducer and second stage.- Usually, in designing a multistage compressor, the inlet hub-tip ratio, the rotational speed, the weight flow, and the inlet total temperature are known. Once an approximate mean-radius pressure ratio is decided upon for the first two stages and an efficiency is assumed, the mean-radius power input for each of these stages is known. When this power input is known, an estimate can be made of the static-temperature increase that will occur in the first two stages. By using the static temperatures, the r_h/r_t for stations 4 and 6 can be obtained from equation (13). Then an approximate curve of r_h/r_t against station can be drawn from station 1 to station 6. The hub-tip ratio corresponding to station 5 may be used as a first approximation for the second stage. By using the power input assumed for this stage and this hub-tip ratio, the stage may be calculated from figure 3 and equation (9). The inducer-stage hub-tip ratio will, as a first approximation, be chosen as that occurring at station 3 on the curve drawn from stations 1 to 4 to 6. The tangential-velocity distribution entering the second rotor V_{u_4} is extrapolated down to this lower hub-tip ratio and equation (4) is used to determine the inducer power-input distribution.

Equation (7) gives the axial-velocity distribution leaving the inducer rotor as a function of the V_{u_3} and V_{u_4} distributions. When either V_{u_2} or V_{u_3} is specified, the other automatically becomes known since $V_{u_3} - V_{u_2} = \Delta W_u$ and the power input has been fixed by the V_{u_4} distribution and the power input at the mean section. As a first

approximation to the most desirable distribution, the V_{u_3} distribution can be chosen equal to the V_{u_5} distribution. This approximation fixes the V_{u_2} distribution and by using equations (6) and (7) the axial-velocity distribution at the inlet and exit of the inducer stage can be calculated. The continuity equation must of course be satisfied. The choice of the V_{u_3} distribution can then be varied in an attempt to obtain the maximum possible rotational speed within the prescribed Mach number and radial-flow limitations. Once the first two stages have been calculated, $\left(r_h/r_t\right)_4$ and $\left(r_h/r_t\right)_6$ can be recalculated by using equation (13), and the curve shown in figure 6 can be redrawn between stations 1 to 6 with new values of hub-tip ratios occurring at stations 3 and 5. By using these values, the first two stages are recalculated until the chosen hub-tip ratios for the inducer and the second stages coincide with those occurring at stations 3 and 5. Two or three trials are usually sufficient if an inducer-stage pressure ratio which is not the maximum pressure ratio possible is acceptable. A high average pressure ratio per stage can then be obtained by increasing the loading in the succeeding stages.

The first- and second-stage Mach numbers and turning angles should be checked. The critical Mach number locations are the rotor tip inlet and the stator hub exit in both stages.

APPLICATION OF DESIGN TECHNIQUE

Design Criteria

Design calculations by means of the preceding technique have been made for several multistage compressors for a range of weight flows at compressor inlet hub-tip ratios of 0.40, 0.50, and 0.60. The following design criteria were adopted for these calculations:

Tip radius: The tip radius was maintained constant for all stage calculations for a given compressor.

Hub radius: The hub radius was increased at such a rate that the area contraction just counterbalanced the density increase and maintained a constant average axial velocity through each compressor. No allowance for boundary layer was made.

Efficiency: The polytropic efficiency (as defined in reference 7) used to calculate the density change and hence the rate of area contraction was chosen as 1.00 at the mean radius. This choice was made because

the use of any efficiency other than 1.00 for the density change would not be consistent with the assumption of a zero radial gradient of entropy and would therefore complicate the analysis greatly. The rate of area contraction was therefore somewhat greater than would occur in an actual compressor.

In order to compare the pressure ratios for this type of design with other designs which have been built and tested, the polytropic efficiency used to calculate pressure ratios was taken as 0.90.

Maximum Mach number: The maximum Mach number of the air flow relative to the blades was taken as 0.75 for all designs. This limitation is conservative except when used with highly cambered blade sections.

Maximum turning angles: For this type of design, maximum turning angles occur at the hub. The solid curves in figure 7 show the turning-angle limitations that were used in this analysis. The choices were based on low-speed cascade data obtained at various cambers for the NACA 65-series compressor blades at solidities of 1.5 and 1.0. These data do not represent absolute maximum turning angles but were somewhat arbitrarily chosen at lower values. The values chosen would permit higher operating Mach numbers and would give a somewhat greater operating range than the absolute maximums. The dashed curves represent the maximum turning angles at each inlet air angle that were obtained at the hub and tip sections in the compressor design calculations. Those points at the tip which exceeded the cascade-data curves at $\sigma = 1.0$ occurred in the last stages of some of the compressors.

Number of stages: The number of stages was limited to that number which gave an exit hub-tip ratio closest to 0.90. From unpublished data obtained at the Lewis Flight Propulsion Laboratory of the NACA, the efficiency appears to decrease considerably above this hub-tip ratio. In reference 9, rotor tests were reported at hub-tip ratios varying from 0.75 to 0.95 and these tests further verified the fact that above a r_h/r_t of 0.90 the efficiency tends to fall considerably.

Range of weight flows: One design was completed for a weight flow of 32.5 pounds per second per square foot of frontal area at an inlet hub-tip ratio of 0.40. In other designs the weight flows were varied from 22.5 to 27.5 and 20.0 to 25.0 pounds per second per square foot of frontal area at inlet hub-tip ratios of 0.50 and 0.60, respectively. The standard sea-level inlet conditions used were stagnation temperature 520° R and stagnation density 0.002378 slug per cubic foot.

Results of Calculations

The axial-velocity distributions calculated for seven combinations of design parameters are presented in tables 1 to 7 and a summary of the design parameters and important results is given in table 8. In order to illustrate the flow characteristics that are inherent in inducer designs, a complete preliminary design for a compressor having an inlet hub-tip ratio of 0.40 and a specific weight flow of 32.5 pounds per second per square foot of frontal area is presented in appendix B. This design is herein denoted as design 1 and its design parameters are presented in table 1.

COMPARISON AND DISCUSSION OF RESULTS

Effects of specific weight flow on design rotational speed.- The design tip rotational speeds used for each of the designs are shown in figure 8. These design rotational speeds were selected to approximate roughly the maximum values associated with each of the weight flows. The curves show that at a constant hub-tip ratio the design rotational speed increased with decreasing specific weight flow. The design rotational speed increased because at lower weight flows, that is, at lower axial velocities, the design rotational speed can be increased and still maintain the same Mach number limitation. Figure 8 also shows that, at a constant design rotational speed, the specific weight flow increased with decreasing inlet hub-tip ratio.

Rate of annulus contraction.- The hub-tip ratios used for the stage-by-stage calculations of the several compressor designs are presented in figure 9. The general shape of the annulus-contraction curve remains about the same for all the designs considered. Since the contraction rate has been set to maintain a constant average axial velocity through each compressor, with η assumed to be constant, a more rapid contraction rate can be expected from the designs having greater over-all pressure ratios, as a comparison of the hub-tip-ratio curves and their corresponding design pressure ratios show.

Effects of weight flow on inlet angles and amount of radial flow.- An examination of the inlet angles in tables 2a, 3, and 4 for designs all having inlet hub-tip ratios of 0.50 shows that, as specific weight flow increased, the design inlet air angles decreased. The tables also show that the amount of radial flow increased as the specific weight flow decreased at a particular inlet hub-tip ratio (from tables 2a and 4, it can be seen that the maximum deviation in axial velocity from the average ranged from 24.8 percent to 55.2 percent when the specific weight flow decreased from 27.5 to 22.5 lb/sec/sq ft frontal area). This trend can be explained by the fact that, as the specific weight flow is

reduced, a greater design rotational speed and therefore a greater power input per stage is permitted within the same Mach number limitation. This increase in permitted power input per stage causes two counteracting effects which can best be seen by an examination of figure 3. The first effect is the increase in the amount of radial flow caused by an increase in power-input ratio per stage at a constant hub-tip ratio; however, as the power input per stage is increased, the density change becomes greater and, in order to maintain a constant axial velocity, the hub contraction rate must be increased. This increase in hub contraction brings about the second effect which is the decrease in radial flow; however, the effect of the increased hub-tip ratio in reducing radial flows is over-balanced by the increase in radial flow associated with the increased power-input ratio. The predominant effect of increased power-input ratio makes the radial flows greater in the designs having lower specific weight flows.

In the later stages where the hub-tip ratio has increased, the difference in the amount of radial flow in designs 2a, 3, and 4 is lessened. This effect is expected since in figure 3 the lines of constant hub-tip ratio become steeper as the hub-tip ratio is increased. Hence, for a fixed amount of power-input-ratio increase, the associated increase in radial flow becomes less as the hub-tip ratio is increased.

In tables 5, 6, and 7, an examination of designs 5, 6, and 7 having inlet hub-tip ratios of 0.60 indicates that all the trends observed in examining the designs having inlet hub-tip ratios of 0.50 are again evident at the higher hub-tip ratio. The same trends probably would occur at inlet hub-tip ratios of 0.40; however, only one design was calculated at that hub-tip ratio.

Design total-pressure ratios.- The ratio of the mean-radius total pressure to the compressor inlet total pressure is given in figures 10 and 11 for inlet hub-tip ratios of 0.50 and 0.60, respectively, for the same number of stages (7). The over-all pressure ratio increases as the specific weight flow decreases. The difference in shape of the curves results from the value of rotational speed selected for each specific weight flow. These pressure ratios might have been raised by increasing the design rotational speed; however, this change would require redesigning the inducer stage to keep within the Mach number limitation.

Effect of hub-tip ratio on amount of radial flow at constant weight flow.- The amount of radial flow decreases as the inlet hub-tip ratio is increased at a constant weight flow. The amount of radial flow in a blade row is indicated by the maximum change in axial velocity across the blade row. For example, when the inlet hub-tip ratio is increased from 0.50 to 0.60 at a constant weight flow (see tables 2a and 6), the amount of

radial flow decreases as indicated by the following decreases in the maximum change in axial velocity in a stage: 55 percent to 22 percent across the inducer stator; 42 percent to 22 percent across the second-stage rotor and stator; 18 percent to 10 percent across the sixth-stage rotor and stator. From these figures, it can be seen that the amount of radial flow is approximately halved as the inlet hub-tip ratio is increased from 0.50 to 0.60 at a constant weight flow.

Effects of design-rotational-speed variation at same weight flow and inlet hub-tip ratio.- In order to determine the effect of a small change in design rotational speed on over-all pressure ratio, designs 2a and 2b were executed. The design tip rotational speeds for designs 2a and 2b were 1,235 feet per second and 1,157 feet per second, respectively. The design rotational speed of design 2a represents an increase of 6.7 percent of the design rotational speed of design 2b. The ratio of mean-radius total pressure to compressor-inlet total pressure plotted against number of stages is given for these designs in figure 12. The higher design rotational speed resulted in somewhat higher Mach numbers in the later stages where the loading limitation was the maximum turning angle permissible. The amount of Mach number increase averaged approximately 0.025. In figure 12, design 2a gave an over-all total-pressure ratio of 6.90 as compared with 6.14 for design 2b. The 6.7-percent increase in design rotational speed resulted in about a 12.4-percent increase in over-all total-pressure ratio. Hence, small increases in design rotational speed do affect the over-all total-pressure ratio enough to change the shape of the curves presented in figures 10 and 11. However, the trend of decreasing pressure ratio with increasing weight flow will not be affected.

Of course, raising the design rotational speed required that the V_{u_3} distribution in the inducer stage be altered to keep the Mach numbers from exceeding 0.75. This change resulted in an increase in radial flow in the inducer stage, that is, greater changes in axial velocity across the inducer stage (see figs. 13 and 14 for velocity diagrams). The greatest axial velocity change in design 2b occurred at the hub section across the inducer stator and was about a 40-percent decrease in axial velocity. By increasing the design rotational speed by 6.7 percent (design 2a), the axial-velocity change at the hub section was increased from 40 percent to 49 percent, representing approximately a 22-percent increase. After the first stage, the axial-velocity change decreases monotonically from about 40 percent in the second stage to about 18 percent in the last stage in both designs. In both designs, the inlet air angles were quite high and increased from stage to stage.

Comparison of the characteristics of the eight designs presented.- From table 8, it can be seen that average total-pressure ratios per stage ranging from 1.28 to 1.38 appear to be attainable. Present-day cascade

and rotor tests indicate that the turning angles required to obtain these high average stage pressure ratios are within the range of efficient highly cambered blade sections.

If the number of stages was limited by keeping the exit hub-tip ratio close to 0.90, the specific power input would increase for each inlet hub-tip ratio with increasing specific weight flow. This change would almost completely be the result of the increased number of stages that could be used as the specific weight flow increased. The specific power input could be increased by decreasing the stage pressure ratios somewhat in the later stages so that one or more additional stages could be used without exceeding the exit hub-tip limitation of 0.90. This increase in stages would raise the over-all total-pressure ratio and, of course, would lower the average total-pressure ratio per stage.

As inlet hub-tip ratio decreased, the specific power input increased. At the same weight flow, the average total-pressure ratio per stage increased as the hub-tip ratio decreased.

Use of design calculations for preliminary design information.- The design studies discussed, in addition to indicating the influence of the variation of the design parameters, may also be used as a source for preliminary design information. They indicate the combinations of design rotational speed, inlet hub-tip ratio, specific weight flow, and power input per unit frontal area that can be used to obtain high pressure ratios per stage. The choice of the combination of design parameters to be used for a particular over-all total-pressure ratio will depend on such factors as the amount of frontal area which can be tolerated in a specific design, the importance which is attached to reducing the compressor length, and the limitations which are placed on the rotational speed.

Résumé of significant design trends.- Calculations made for specific multistage compressor designs indicate the following trends:

(A) Trends for Over-all Compressor

(a) Average pressure ratios per stage varying from 1.28 to 1.38 are attainable at inlet hub-tip ratios of 0.40, 0.50, and 0.60 with weight flows ranging from 20.0 to 32.5 pounds per second per square foot of frontal area.

(b) The design rotational speed increased with decreasing specific weight flow at a constant inlet hub-tip ratio.

(c) The weight flow increased with decreasing inlet hub-tip ratio at a constant design rotational speed.

(d) The amount of radial flow increased as the specific weight flow decreased at a constant inlet hub-tip ratio.

(e) The amount of radial flow is sharply reduced as the inlet hub-tip ratio is increased from 0.50 to 0.60 at a constant weight flow.

(f) A rather large increase in amount of radial flow and over-all total-pressure ratio resulted from a small increase in design rotational speed at a constant weight flow.

(g) Stage inlet air angles increased from stage to stage in all designs.

(h) Stage inlet air angles increased as specific weight flow decreased at each inlet hub-tip ratio.

(B) Trends for All Stages Following the Inducer Stage

(a) The amount of radial flow decreased with increasing hub-tip ratio at a constant power-input ratio.

(b) The amount of radial flow increased as the power-input ratio increased at a constant hub-tip ratio.

(c) The amount of radial flow decreased with increasing hub-tip ratio, power-input ratio, and hub inlet air angle at a constant hub turning angle and tip-rotational-speed ratio.

(d) The power-input ratio, amount of radial flow, and hub inlet air angle all increased as the tip-rotational-speed ratio increased at a constant hub turning angle and hub-tip ratio.

CONCLUDING REMARKS

A summary of the significant conclusions which result from the analysis and calculations of the solid-body inducer compressor design is as follows:

1. Simplified, general, three-dimensional compressible-flow equations were derived, which permitted the axial velocity distributions at any station between blade rows to be calculated. These equations were applied to the inducer compressor design.

2. A general chart of power-input ratio plotted against hub axial velocity ratio, which satisfies continuity for various hub-tip ratios, is presented This chart facilitates design calculation for all stages

following the inducer stage regardless of the combination of design rotational speed, inlet axial velocity, and inlet total temperature specified.

3. A method is presented of plotting curves of constant hub turning angle on the general chart for any particular rotational-speed ratio. These curves facilitate stage design calculations when the limitation on loading is turning angle.

4. A method is presented of plotting curves of constant inlet air angle on this general chart for any particular rotational-speed ratio. These curves aid in the selection of power-input values in regions where the variation of hub-turning-angle limitation with inlet air angle is important.

5. Calculations made for specific multistage compressor designs indicated that, at inlet hub-tip ratios of 0.40, 0.50, and 0.60 with weight flows ranging from 20.0 to 32.5 pounds per second per square foot of frontal area, average pressure ratios per stage varying from 1.28 to 1.38 are attainable.

6. From these calculations some of the effects of specific weight flow, rotational speed, hub-tip ratio, turning angle, and inlet air angle on power input, amount of radial flow, and over-all total-pressure ratio are investigated.

Langley Aeronautical Laboratory
National Advisory Committee for Aeronautics
Langley Field, Va., September 19, 1951

APPENDIX A

DETERMINATION OF SIMPLIFIED, THREE-DIMENSIONAL, COMPRESSIBLE-FLOW EQUATIONS FOR COMPRESSOR STAGE

General Equations for Rotor, Stator, and Guide Vane

Axial-velocity distribution behind a rotor.- If positions x and y are assumed to be anywhere along the radius,

$$t_y = T_{y_s} - \frac{V_y^2}{2c_p}$$

$$t_x = T_{x_s} - \frac{V_x^2}{2c_p}$$

or

$$t_y - t_x = T_{y_s} - T_{x_s} - \frac{V_y^2}{2c_p} + \frac{V_x^2}{2c_p} \tag{A1}$$

If simplified radial equilibrium is assumed,

$$\int_{p_x}^{p_y} \frac{dp}{\rho} = \int_{r_x}^{r_y} \frac{V_u^2}{r}\, dr \tag{A2}$$

The fundamental energy equation states that

$$\frac{dp}{\rho} = c_p\, dt - t\, ds \tag{A3}$$

Combining equations (A2) and (A3) and integrating results in

$$t_y - t_x = \frac{1}{c_p}\left(\int_{r_x}^{r_y} \frac{V_u^2}{r}\, dr + \int_{s_x}^{s_y} t\, ds\right) \tag{A4}$$

Equating equations (A1) and (A4) results in

$$T_{y_s} - T_{x_s} - \frac{V_y^2}{2c_p} + \frac{V_x^2}{2c_p} = \frac{1}{c_p}\left(\int_{r_x}^{r_y} \frac{V_u^2}{r}\,dr + \int_{s_x}^{s_y} t\,ds\right) \tag{A5}$$

If the displacement of a streamline is small through one blade row, then

$$\left.\begin{aligned} T_{y_{s_e}} - T_{y_{s_i}} &= \frac{U_y\,\Delta W_{u_y}}{c_p} \\ T_{x_{s_e}} - T_{x_{s_i}} &= \frac{U_x\,\Delta W_{u_x}}{c_p} \end{aligned}\right\} \tag{A6}$$

Writing equation (A5) for the exit e and substituting from equations (A6) results in

$$T_{y_{s_i}} - T_{x_{s_i}} + \frac{U_y\,\Delta W_{u_y} - U_x\,\Delta W_{u_x}}{c_p} - \frac{V_{y_e}^2}{2c_p} + \frac{V_{x_e}^2}{2c_p} =$$

$$\frac{1}{c_p}\left(\int_{r_x}^{r_y} \frac{V_{u_e}^2}{r}\,dr + \int_{s_x}^{s_y} t_e\,ds\right) \tag{A7}$$

Writing equation (A5) for the inlet i and subtracting it from equation (A7) results in

$$V_{y_e}^2 = V_{x_e}^2 + \left(2U_y\,\Delta W_{u_y} + V_{y_i}^2\right) - \left(2U_x\,\Delta W_{u_x} + V_{x_i}^2\right) - 2\int_{r_x}^{r_y} \frac{V_{u_e}^2}{r}\,dr +$$

$$2\int_{r_x}^{r_y} \frac{V_{u_i}^2}{r}\,dr - 2\int_{s_x}^{s_y} t_e\,ds + 2\int_{s_x}^{s_y} t_i\,ds \tag{A8}$$

For convenience, let station x be the mean-radius section and let station y be any other station to be examined. Then, by replacing the velocities by their components, equation (A8) becomes

$$V_{a_e}^2 = V_{a_{e_m}}^2 + \left(2U\,\Delta W_u + V_{a_i}^2 + V_{u_i}^2 - V_{u_e}^2\right) - \left(2U_m\,\Delta W_{u_m} + V_{a_{i_m}}^2 + V_{u_{i_m}}^2 - V_{u_{e_m}}^2\right) + 2\int_{r_m}^{r}\frac{V_{u_i}^2}{r}\,dr - 2\int_{r_m}^{r}\frac{V_{u_e}^2}{r}\,dr + 2\int_{s_m}^{s} t_i\,ds - 2\int_{s_m}^{s} t_e\,ds \qquad (A9)$$

If constant entropy along the radius is assumed, then equation (A9) becomes

$$V_{a_e}^2 = V_{a_{e_m}}^2 + \left(2U\,\Delta W_u + V_{a_i}^2 + V_{u_i}^2 - V_{u_e}^2\right) - \left(2U_m\,\Delta W_{u_m} + V_{a_{i_m}}^2 + V_{u_{i_m}}^2 - V_{u_{e_m}}^2\right) + 2\int_{r_m}^{r}\frac{V_{u_i}^2}{r}\,dr - 2\int_{r_m}^{r}\frac{V_{u_e}^2}{r}\,dr \qquad (A10)$$

Equation (A10) gives the axial-velocity distribution necessary for equilibrium behind a rotor as a function of the conditions ahead of the rotor, the power-input distribution, and the tangential-velocity distribution behind the rotor. It does not include continuity.

Axial-velocity distribution behind a stator.- The power-input term, $U\,\Delta W_u$, drops out of equation (A10) when it is used across a stationary blade row. The equation becomes

$$V_{a_e}^2 = V_{a_{e_m}}^2 + \left(V_{a_i}^2 + V_{u_i}^2 - V_{u_e}^2\right) - \left(V_{a_{i_m}}^2 + V_{u_{i_m}}^2 - V_{u_{e_m}}^2\right) + 2\int_{r_m}^{r}\frac{V_{u_i}^2}{r}\,dr - 2\int_{r_m}^{r}\frac{V_{u_e}^2}{r}\,dr \qquad (A11)$$

Axial-velocity distribution behind a guide vane.- For a guide vane, the inlet axial velocity is constant and there are no entering tangential components; hence, equation (A10) becomes

$$V_{a_e}^2 = V_{a_{e_m}}^2 + V_{u_{e_m}}^2 - V_{u_e}^2 - 2\int_{r_m}^{r} \frac{V_{u_e}^2}{r}\,dr \tag{A12}$$

Equations for Inducer-Type Design

Inducer-stage power-input distribution.- A certain radial total-temperature distribution must be set up by the first stage in order to make the rotor inlet axial velocity constant for the second rotor. The derivation of the required power-input distribution for the inducer stage is as follows:

Replacing stations i and e in equation (A11) by stations 3 and 4 and assuming V_{a_4} is constant from hub to tip results in

$$V_{a_{3_m}}^2 = V_{a_3}^2 + \left(V_{u_3}^2 - V_{u_{3_m}}^2\right) + \left(V_{u_{4_m}}^2 - V_{u_4}^2\right) +$$

$$2\int_{r_m}^{r} \frac{V_{u_3}^2}{r}\,dr - 2\int_{r_m}^{r} \frac{V_{u_4}^2}{r}\,dr \tag{A13}$$

If equation (A10) is written for stations 2 and 3 and equation (A13) is substituted, it follows that

$$2U\,\Delta W_u - 2U_m\,\Delta W_{u_m} + V_{a_2}^2 - V_{a_{2_m}}^2 + V_{u_2}^2 - V_{u_{2_m}}^2 + V_{u_{4_m}}^2 - V_{u_4}^2 +$$

$$2\int_{r_m}^{r} \frac{V_{u_2}^2}{r}\,dr - 2\int_{r_m}^{r} \frac{V_{u_4}^2}{r}\,dr = 0 \tag{A14}$$

Writing equation (A12) for stations 1 and 2 and substituting into equation (A14) results in

$$U\,\Delta W_u = U_m\,\Delta W_{u_m} + \frac{V_{u_4}^2 - V_{u_{4_m}}^2}{2} + \int_{r_m}^{r} \frac{V_{u_4}^2}{r}\,dr \tag{A15}$$

Equation (A15) gives the inducer-stage power-input distribution necessary to set up constant inlet axial velocity for the second-stage rotor.

Axial-velocity distribution behind rotors succeeding the inducer stage.- The radial total-temperature distribution required to make the axial-velocity distribution entering the second-stage rotor radially constant was derived previously (equation (A6)). It is assumed that the axial-velocity distribution entering all rotors after the second stage can be made constant by making the radial power-input distribution constant for all the rotors after the inducer stage. In order to have velocity diagrams which were symmetrical in the tangential direction $V_{u_{av}}$ was chosen proportional to r.

Rewriting the general rotor equation (equation (A10)) for the conditions of $U\,\Delta W_u = \text{Constant}$, $V_{u_{av}} \propto r$, and $V_{a_i} = \text{Constant}$ gives

$$V_{a_e}^2 = V_{a_{e_m}}^2 + \left(V_{u_i}^2 - V_{u_e}^2\right) - \left(V_{u_{i_m}}^2 - V_{u_{e_m}}^2\right) + 2\int_{r_m}^{r} \frac{V_{u_i}^2}{r}\,dr - 2\int_{r_m}^{r} \frac{V_{u_e}^2}{r}\,dr \tag{A16}$$

Since for a symmetrical velocity diagram $U = V_{u_e} + V_{u_i}$ and by definition $\Delta W_u = V_{u_e} - V_{u_i}$, the assumption that $U\,\Delta W_u$ is constant radially results in

$$U\,\Delta W_u = V_{u_{e_m}}^2 - V_{u_{i_m}}^2 = V_{u_e}^2 - V_{u_i}^2 = \text{Constant} \tag{A17}$$

Substituting equation (A17) into equation (A16) results in

$$V_{a_e}^2 = V_{a_{e_m}}^2 - 2U\,\Delta W_u \int_{r_m}^{r} \frac{dr}{r} \tag{A18}$$

Performing the integration results in

$$V_{a_e}^2 = V_{a_{e_m}}^2 - 2U\,\Delta W_u \log_e \frac{r}{r_m} \tag{A19}$$

Equation (A19) yields the equation for the axial-velocity distribution behind a rotor having constant power-input distribution, constant inlet axial-velocity distribution, and having the average tangential velocity proportional to the radius.

APPENDIX B

DETAILS OF A TYPICAL PRELIMINARY COMPRESSOR DESIGN

Design 1 will be used as an example to present the details of a typical preliminary design calculation. The design parameters for design 1 are included in table 1.

The Mach number limitation was chosen as 0.75 and the limiting turning angle was chosen as 38.0° for this design. Since the resulting inlet air angles were all about 50.0° or less, this turning angle is within the limits of cascade and rotor test results for efficient blade-section performance.

The hub shape of design 1 is presented in figure 9 with the effect of boundary layer being neglected.

Velocity diagrams for all stages at hub, mean-radius, and tip sections are presented in figure 15. In all stages other than the first or inducer stage, these diagrams are symmetrical in the tangential direction. The passage was assumed to have no taper for each stage calculation.

The radial flows were not excessive. The maximum percentage change in axial velocity occurred across the inducer stator hub and was 28.7 percent. The over-all total-pressure ratio obtained was 5.73 for a seven-stage design which is equivalent to an average stage pressure ratio of 1.28.

The Mach numbers entering the rotors and the stators are presented in figure 16(a). The limitation on loading in the first four stages was the Mach number entering the stator hub. The Mach number limitation persisted in this design because of the high weight flow. After the fourth stage, the amount of loading was restricted by the turning-angle limitation and as a result the Mach numbers for stations 10 to 15 decreased. In this design the rate of annulus contraction was fixed to maintain a constant average axial velocity through the compressor.

The velocities relative to the rotors are presented in figure 16(b); the velocities relative to the stators, in figure 16(c); the axial velocities, in figure 16(d); and the tangential velocities, in figure 16(e). The relative velocities entering the rotors generally increase with radius; those leaving the rotors decrease with radius. The absolute velocities entering the stators decrease with radius; those leaving the stators increase with radius.

The percentage change in axial velocity across a blade row varies from 28.7 in the first-stage stator to 9.5 percent in the seventh-stage stator and rotor. The relative velocities entering the rotors and the absolute velocities entering the stators are increased in successive stages to maintain the high Mach numbers as the air temperature increases. These velocity increases result because the power input is increased in the succeeding stages until the limiting turning angle is reached. The tangential components of absolute velocities (fig. 16(e)) generally increase with radius for each hub-tip ratio. In successive stages, the rotor inlet tangential components of absolute velocities decrease; as a result, the relative rotor inlet velocities increase. The stator inlet tangential components of absolute velocities increase in successive stages; as a result, the stator inlet absolute velocities increase.

The static-pressure ratios across successive stages at the various radial positions are plotted in figure 16(f). The hub value of hub-tip ratio used for each stage was that occurring between the rotor and stator of that stage. The static pressures are very nearly constant with respect to radius.

REFERENCES

1. Hall, R. S.: Aerodynamic Problems in Axial Compressors for Aircraft Jet Engines. Preprint No. 216, Inst. Aero. Sci.

2. Soderberg, C. Richard: The Choice of Pressure Ratio in Aircraft Gas Turbine Power Plants. Preprint No. 218, Inst. Aero. Sci.

3. Kahane, A.: Investigation of Axial-Flow Fan and Compressor Rotors Designed for Three-Dimensional Flow. NACA TN 1652, 1948.

4. Wu, Chung-Hua, and Wolfenstein, Lincoln: Application of Radial-Equilibrium Condition to Axial-Flow Compressor and Turbine Design. NACA Rep. 955, 1950. (Formerly NACA TN 1795.)

5. Bowen, John T., Sabersky, Rolf H., and Rannie, W. Duncan: Theoretical and Experimental Investigations of Axial Flow Compressors. Summary Report, Jan. 1949 and Part II, Contract N6-ORI-102 Task Order IV, Office of Naval Res., Mech. Eng. Lab., C.I.T., July 1949.

6. Wu, Chung-Hua, Sinnette, John T., Jr., and Forrette, Robert E.: Theoretical Effect of Inlet Hub-Tip-Radius Ratio and Design Specific Mass Flow on Design Performance of Axial-Flow Compressors. NACA TN 2068, 1950.

7. Sinnette, John T., Jr.: Analysis of Effect of Basic Design Variables on Subsonic Axial-Flow-Compressor Performance. NACA Rep. 901, 1948.

8. Carter, A. D. S.: Three Dimensional Flow Theories for Axial Compressors and Turbines. National Gas Turbine Establishment Rep. No. R.37, Ministry of Supply, Sept. 1948.

9. Eckert, B., Pfluger, F., and Weinig, F.: The Influence of Physical Dimensions (Such as Hub:Tip Ratio, Clearance, Blade Shape) and Flow Conditions (Such as Reynolds Number and Mach Number) on Compressor Characteristics. Part B - The Influence of the Diameter Ratio on the Characteristics Diagram of the Axial Compressor. Vol. 3, BUSHIPS 338, Navy Dept., May 1946.

TABLE 1

DESIGN 1

$\frac{U_t}{V_{a_1}} = 1.684$ $\qquad \frac{w}{A_f} = 32.5 \frac{lb}{sec\text{-}sq\ ft}$

$V_{a_1} = 581.1 \frac{ft}{sec}$ $\qquad \left(\frac{r_h}{r_t}\right)_1 = 0.40$

Stage n	Position	β (deg)	θ (deg)	$\frac{V_{a_{2n}}}{V_{a_1}}$	$\frac{V_{a_{2n+1}}}{V_{a_1}}$
1	h	30.1	21.0	1.153	1.287
	m	37.1	14.7	1.038	1.040
	t	52.0	11.5	.814	.742
2	h	37.7	31.7	1.000	1.210
	m	41.3	18.9		1.019
	t	45.4	7.5		.852
3	h	42.1	33.2	1.000	1.186
	m	44.1	22.1		1.014
	t	47.1	11.5		.850
4	h	45.7	36.7	1.000	1.174
	m	47.0	26.8		1.008
	t	48.8	16.3		.842
5	h	48.2	37.8	1.000	1.147
	m	49.1	29.8		1.006
	t	50.1	21.1		.864
6	h	49.8	38.0	1.000	1.117
	m	50.5	31.6		1.004
	t	51.0	24.5		.887
7	h	50.9	38.0	1.000	1.095
	m	51.4	33.0		1.001
	t	51.8	27.3		.905

NACA

TABLE 2

DESIGNS 2

(a) Design 2a

$\frac{U_t}{V_{a_1}} = 2.933$ $\qquad \frac{w}{A_f} = 22.5 \frac{lb}{sec\text{-}sq\ ft}$

$V_{a_1} = 421.0 \frac{ft}{sec}$ $\qquad \left(\frac{r_h}{r_t}\right)_1 = 0.50$

Stage n	Position	β (deg)	θ (deg)	$\frac{V_{a_{2n}}}{V_{a_1}}$	$\frac{V_{a_{2n+1}}}{V_{a_1}}$
1	h	35.0	21.5	1.371	1.493
	m	52.5	15.0	1.076	1.081
	t	73.6	3.6	.541	.448
2	h	54.2	37.3	1.000	1.418
	m	57.0	18.9		1.044
	t	60.1	-2.5		.600
3	h	58.0	37.5	1.000	1.369
	m	60.0	22.0		1.034
	t	61.6	1.8		.620
4	h	61.1	35.8	1.000	1.285
	m	62.0	24.8		1.022
	t	63.0	9.1		.702
5	h	62.2	34.8	1.000	1.226
	m	62.9	25.4		1.022
	t	63.5	13.4		.758
6	h	63.1	33.6	1.000	1.179
	m	63.5	26.1		1.009
	t	64.0	16.9		.815

NACA

TABLE 2 - Concluded

(b) Design 2b

$\frac{U_t}{V_{a_1}} = 2.750$ $\qquad \frac{w}{A_f} = 22.5 \frac{lb}{sec\text{-}sq\ ft}$

$V_{a_1} = 421.0 \frac{ft}{sec}$ $\qquad \left(\frac{r_h}{r_t}\right)_1 = 0.50$

Stage n	Position	β (deg)	θ (deg)	$\frac{V_{a_{2n}}}{V_{a_1}}$	$\frac{V_{a_{2n+1}}}{V_{a_1}}$
1	h	36.3	23.5	1.295	1.403
	m	52.1	15.7	1.050	1.040
	t	69.0	9.0	.682	.661
2	h	52.2	36.0	1.000	1.381
	m	54.8	18.0		1.034
	t	58.6	-.5		.644
3	h	56.0	38.0	1.000	1.363
	m	58.2	22.4		1.035
	t	60.5	3.2		.644
4	h	59.5	38.0	1.000	1.287
	m	60.6	25.8		1.015
	t	61.6	9.8		.688
5	h	60.8	37.0	1.000	1.230
	m	61.6	26.7		1.020
	t	62.2	48.4		.750
6	h	62.0	35.3	1.000	1.179
	m	62.4	27.5		1.008
	t	62.7	18.0		.814

NACA

TABLE 3

DESIGN 3

$\frac{U_t}{V_{a_1}} = 2.481$ $\qquad \frac{w}{A_f} = 24.7 \frac{lb}{sec\text{-}sq\ ft}$

$V_{a_1} = 470.0 \frac{ft}{sec}$ $\qquad \left(\frac{r_h}{r_t}\right)_1 = 0.50$

Stage n	Position	β (deg)	θ (deg)	$\frac{V_{a_{2n}}}{V_{a_1}}$	$\frac{V_{a_{2n+1}}}{V_{a_1}}$
1	h	33.5	19.8	1.258	1.321
	m	48.7	14.0	1.050	1.040
	t	66.0	11.2	.712	.711
2	h	50.4	36.0	1.000	1.326
	m	53.0	19.8		1.025
	t	56.6	2.0		.704
3	h	54.1	37.9	1.000	1.303
	m	55.8	23.8		1.020
	t	58.0	7.2		.699
4	h	57.4	37.1	1.000	1.233
	m	58.2	28.0		1.015
	t	59.3	13.5		.768
5	h	59.0	37.7	1.000	1.191
	m	59.8	28.8		1.005
	t	60.2	17.8		.796
6	h	60.2	37.0	1.000	1.147
	m	60.5	30.0		1.005
	t	60.9	22.5		.851

NACA

TABLE 4

DESIGN 4

$\frac{U_t}{V_{a_1}} = 1.821$ $\frac{w}{A_f} = 27.5 \frac{lb}{sec\text{-}sq\ ft}$

$V_{a_1} = 539.5 \frac{ft}{sec}$ $\left(\frac{r_h}{r_t}\right)_1 = 0.50$

Stage n	Position	β (deg)	θ (deg)	$\frac{V_{a_{2n}}}{V_{a_1}}$	$\frac{V_{a_{2n+1}}}{V_{a_1}}$
1	h	32.5	25.8	1.130	1.248
	m	42.5	19.7	1.020	1.025
	t	55.2	14.0	.872	.820
2	h	44.1	36.2	1.000	1.230
	m	46.2	23.1		1.015
	t	49.2	9.5		.806
3	h	47.0	36.5	1.000	1.207
	m	48.5	25.5		1.010
	t	50.5	14.8		.826
4	h	49.9	36.9	1.000	1.155
	m	50.6	28.3		1.005
	t	51.8	18.9		.850
5	h	51.2	36.5	1.000	1.125
	m	52.0	30.0		1.005
	t	52.6	22.3		.880
6	h	52.4	37.4	1.000	1.117
	m	53.0	31.6		.995
	t	53.5	26.4		.910
7	h	53.5	38.0	1.000	1.085
	m	54.0	33.6		1.000
	t	54.3	28.9		.913

NACA

TABLE 5

DESIGN 5

$\frac{U_t}{V_{a_1}} = 2.433$ $\frac{w}{A_f} = 20.0 \frac{lb}{sec\text{-}sq\ ft}$

$V_{a_1} = 442.0 \frac{ft}{sec}$ $\left(\frac{r_h}{r_t}\right)_1 = 0.60$

Stage n	Position	β (deg)	θ (deg)	$\frac{V_{a_{2n}}}{V_{a_1}}$	$\frac{V_{a_{2n+1}}}{V_{a_1}}$
1	h	44.5	25.4	1.178	1.318
	m	53.5	23.0	1.020	1.040
	t	64.0	5.0	.815	.591
2	h	53.0	36.8	1.000	1.292
	m	54.8	22.2		1.020
	t	57.5	5.9		.716
3	h	56.0	37.0	1.000	1.250
	m	57.2	25.3		1.015
	t	58.5	11.0		.750
4	h	58.5	36.8	1.000	1.192
	m	59.0	28.1		1.010
	t	59.7	17.2		.808
5	h	59.4	36.5	1.000	1.155
	m	60.0	29.3		1.005
	t	60.5	20.9		.841

NACA

TABLE 6

DESIGN 6

$\frac{U_t}{V_{a_1}} = 1.903$ $\frac{w}{A_f} = 22.5 \frac{lb}{sec\text{-}sq\ ft}$

$V_{a_1} = 511.3 \frac{ft}{sec}$ $\left(\frac{r_h}{r_t}\right)_1 = 0.60$

Stage n	Position	β (deg)	θ (deg)	$\frac{V_{a_{2n}}}{V_{a_1}}$	$\frac{V_{a_{2n+1}}}{V_{a_1}}$
1	h	38.2	27.0	1.112	1.223
	m	47.0	21.4	1.015	1.015
	t	56.1	56.1	.884	.806
2	h	47.5	37.1	1.000	1.220
	m	49.1	24.8		1.010
	t	51.7	12.5		.806
3	h	50.0	35.5	1.000	1.175
	m	51.3	26.2		1.010
	t	52.0	14.4		.840
4	h	51.6	35.5	1.000	1.135
	m	52.5	27.5		1.005
	t	53.0	20.5		.870
5	h	53.1	36.6	1.000	1.113
	m	53.8	30.6		1.000
	t	54.2	23.8		.882
6	h	54.1	37.3	1.000	1.095
	m	54.4	32.3		1.000
	t	55.0	26.9		.901

NACA

TABLE 7

DESIGN 7

$\frac{U_t}{V_{a_1}} = 1.423$ $\frac{w}{A_f} = 25.0 \frac{lb}{sec\text{-}sq\ ft}$

$V_{a_1} = 588.8 \frac{ft}{sec}$ $\left(\frac{r_h}{r_t}\right)_1 = 0.60$

Stage n	Position	β (deg)	θ (deg)	$\frac{V_{a_{2n}}}{V_{a_1}}$	$\frac{V_{a_{2n+1}}}{V_{a_1}}$
1	h	28.2	23.1	1.060	1.111
	m	37.3	17.5	1.000	.995
	t	46.5	13.5	.955	.938
2	h	40.8	34.9	1.000	1.145
	m	42.1	23.6		1.006
	t	44.0	16.2		.875
3	h	44.0	37.7	1.000	1.128
	m	44.8	30.0		1.004
	t	46.0	22.4		.883
4	h	45.5	37.7	1.000	1.102
	m	46.2	31.8		1.003
	t	47.0	25.5		.904
5	h	46.5	37.6	1.000	1.084
	m	47.0	32.7		1.002
	t	47.6	27.9		.924
6	h	47.2	37.4	1.000	1.070
	m	47.6	33.6		1.003
	t	48.0	29.3		.935
7	h	47.7	37.4	1.000	1.060
	m	48.1	34.0		1.003
	t	48.4	30.7		.946

NACA

TABLE 8

SUMMARY OF DESIGN PARAMETERS AND IMPORTANT RESULTS

Design numbers	Inlet hub-tip ratio	Specific weight flow (lb/sec/sq ft frontal area)	Tip-rotational-speed ratio	Inlet axial velocity (ft/sec)	Specific power input hp/sq ft frontal area)	Number of stages	Over-all total-pressure ratio	Average total-pressure ratio per stage
1	0.40	32.5	1.684	581.1	4240	7	5.73	1.28
2a	.50	22.5	2.933	421.0	3360	6	6.90	1.38
2b	.50	22.5	2.750	421.0	3090	6	6.14	1.35
3	.50	24.7	2.481	470.0	3570	6	6.58	1.37
4	.50	27.5	1.821	539.5	3980	7	6.60	1.31
5	.60	20.0	2.453	442.0	2170	5	4.54	1.35
6	.60	22.5	1.903	511.3	2750	6	5.26	1.32
7	.60	25.0	1.423	588.8	3170	7	5.52	1.28

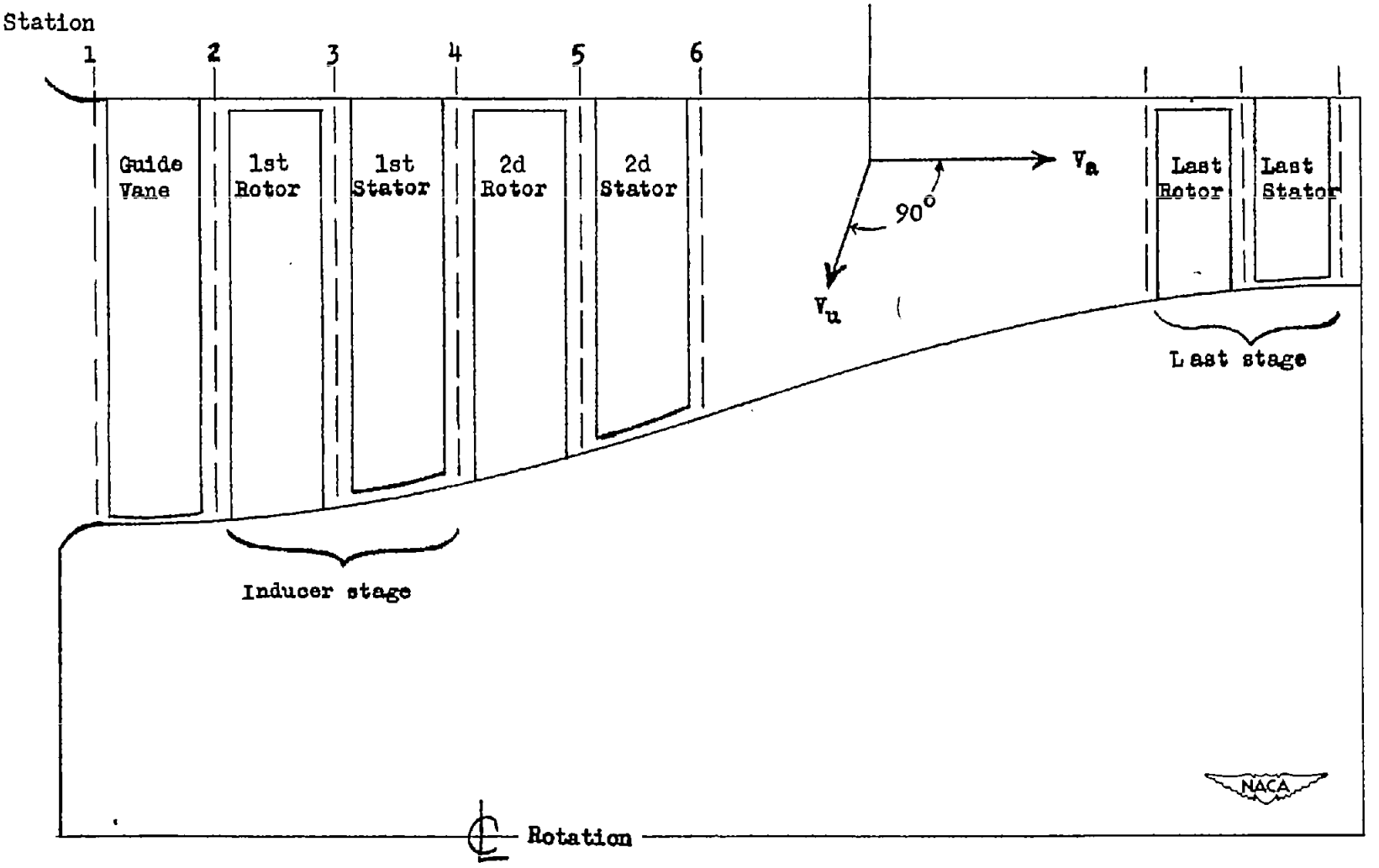

Figure 1.- Coordinate system and station locations.

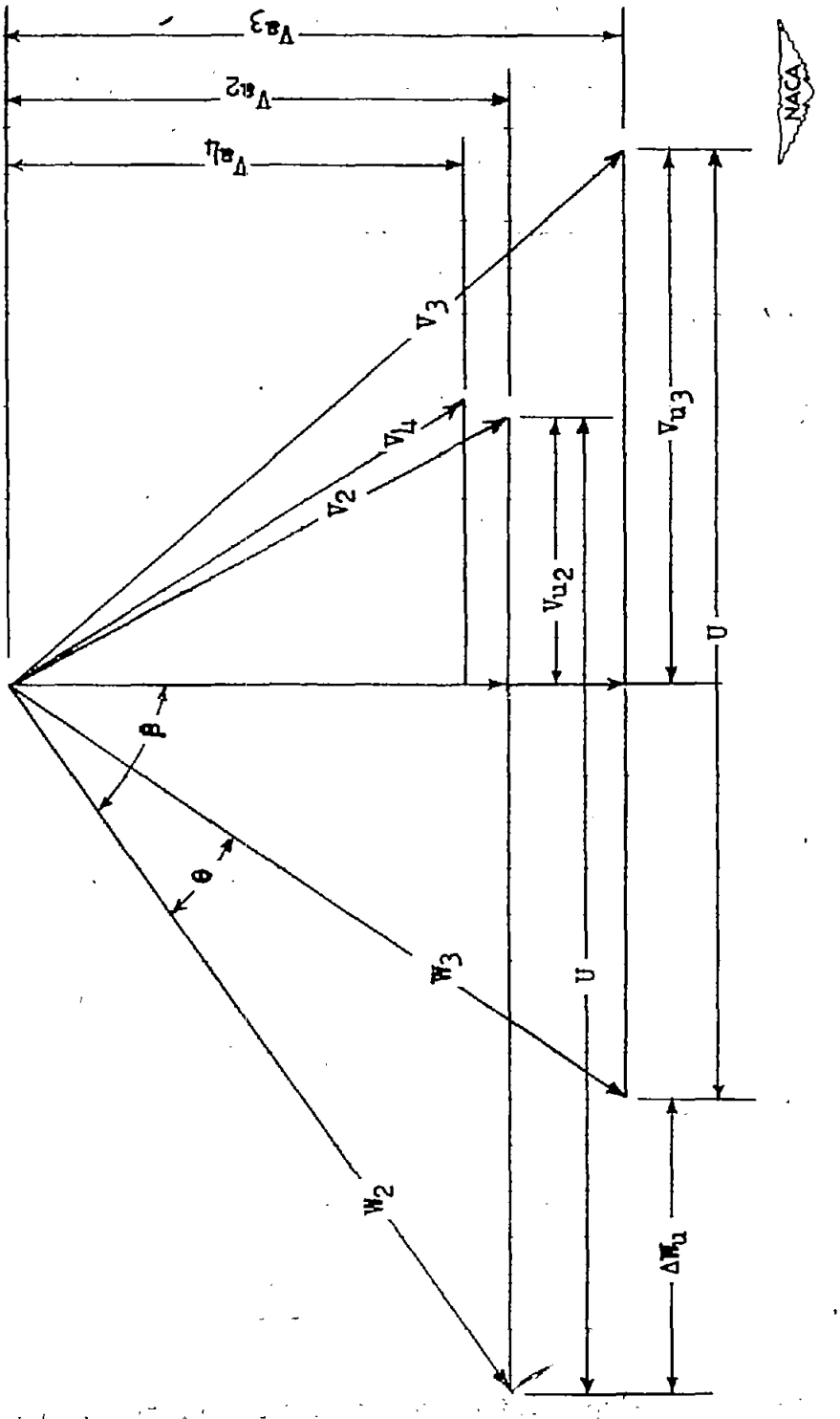

Figure 2.- Vector diagram for a typical compressor stage indicating the symbols used for the velocities and their directions.

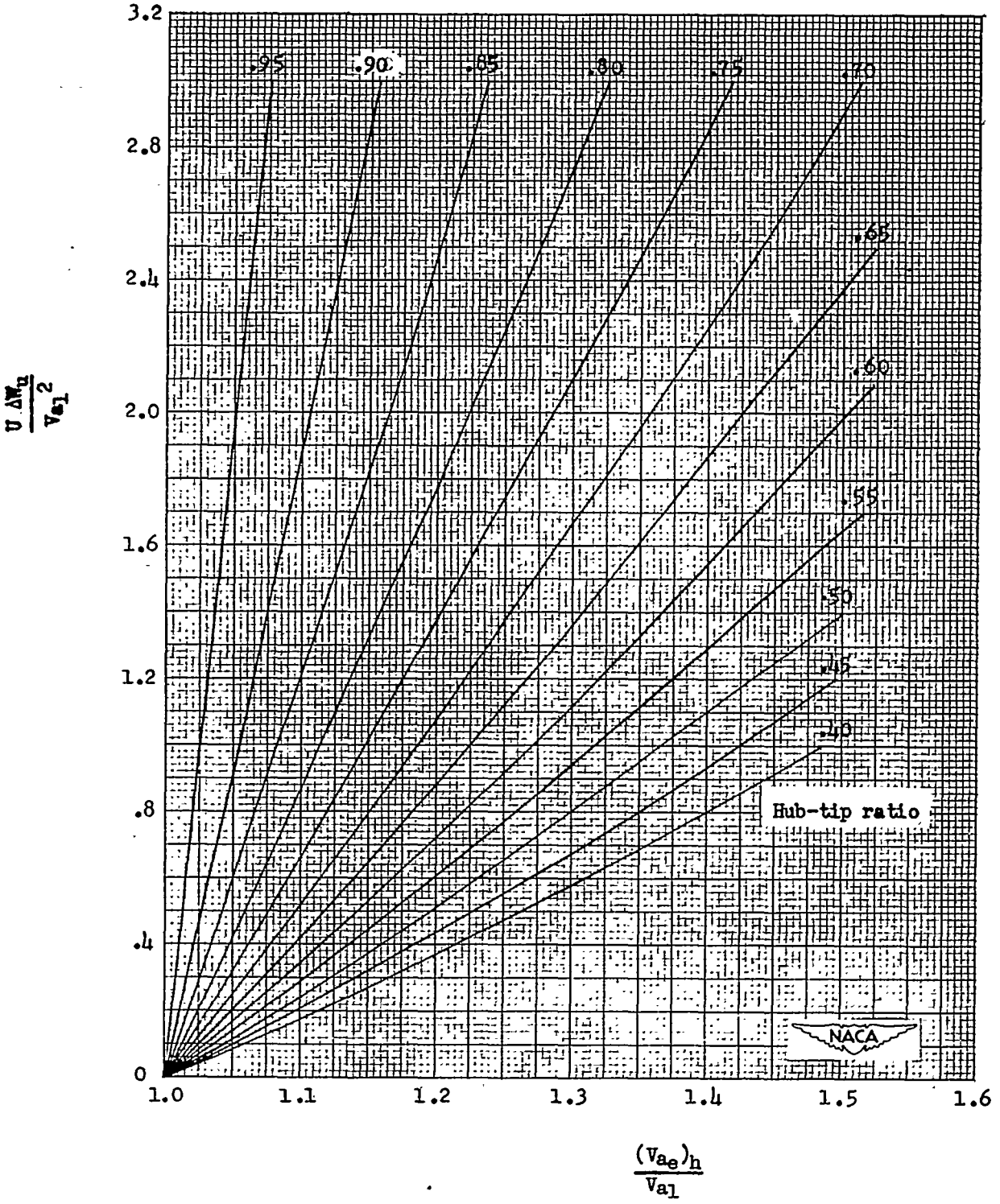

Figure 3.- Stage power-input ratio, for stages following the inducer stage, plotted against the hub-exit axial-velocity ratio which satisfies the continuity equation, for various hub-tip ratios.

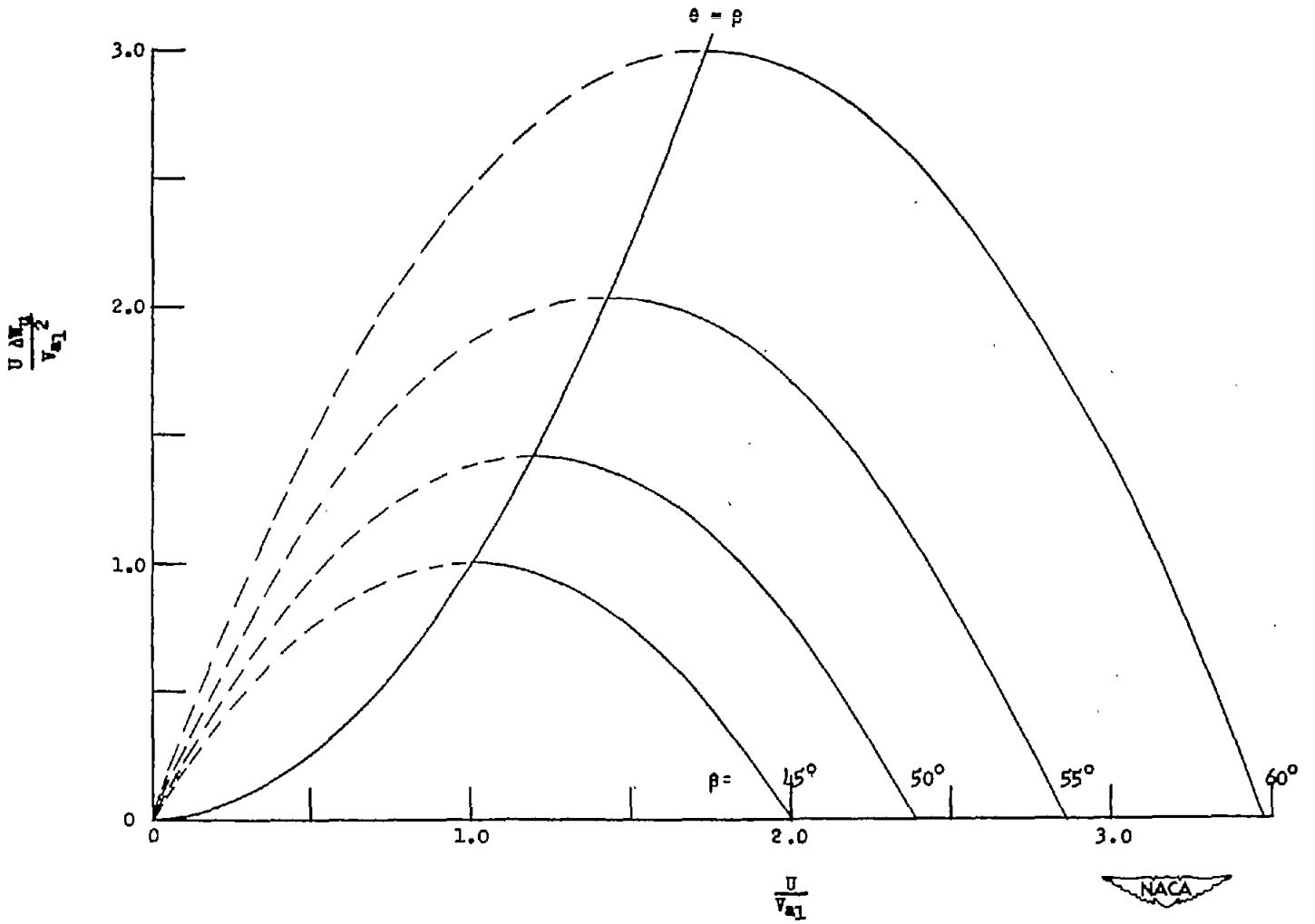

Figure 4.- Stage power-input ratio, for stages following the inducer stage, plotted against the rotational-speed ratio for various air inlet angles.

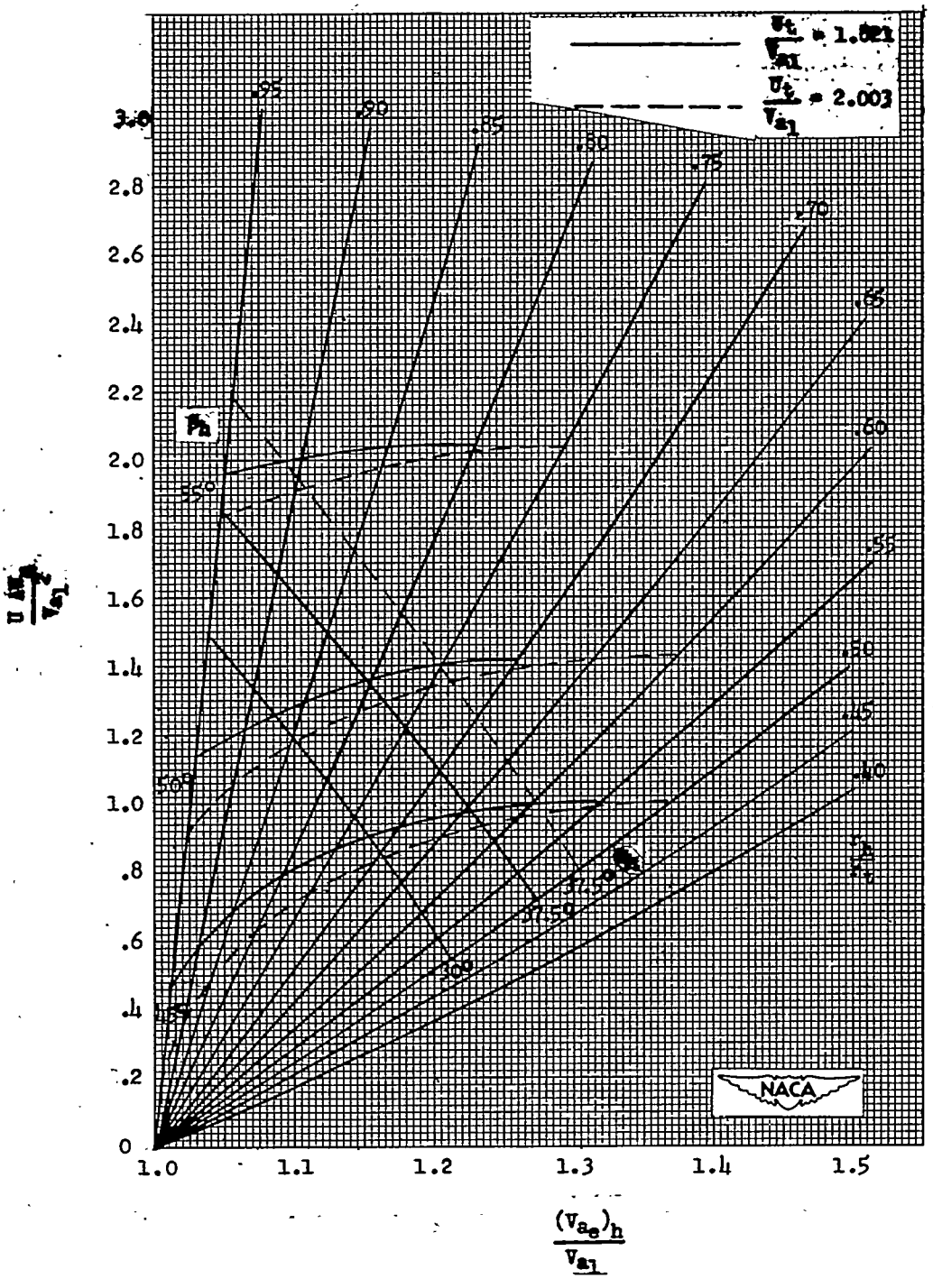

Figure 5.- Curves of constant hub turning and inlet air angles at two tip-rotational-speed ratios superposed on the chart of stage power-input ratio, for stages following the inducer stage, plotted against the hub-exit axial-velocity ratio which satisfies continuity for various hub-tip ratios.

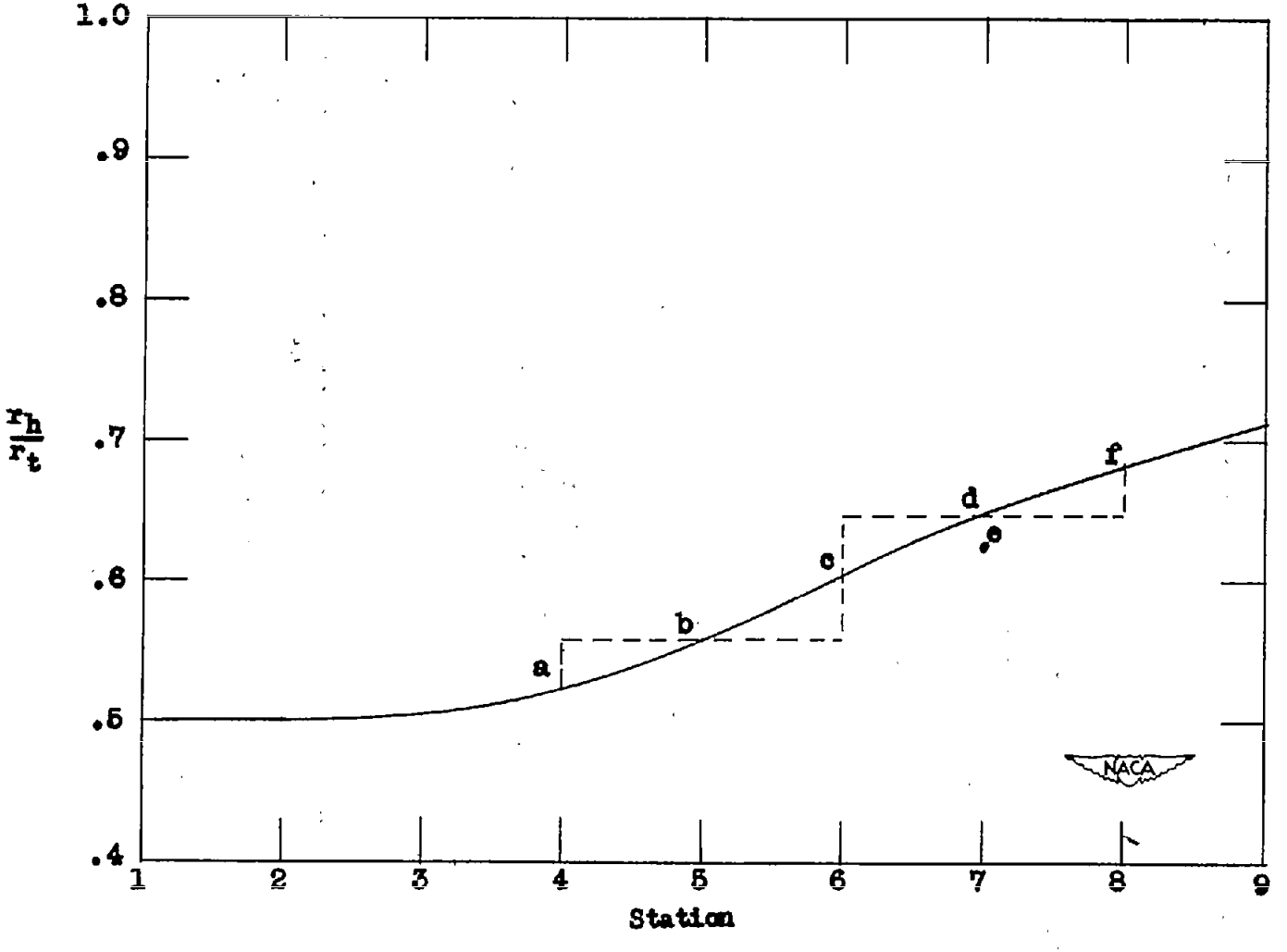

Figure 6.- Hub contour plotted against station between blade rows.

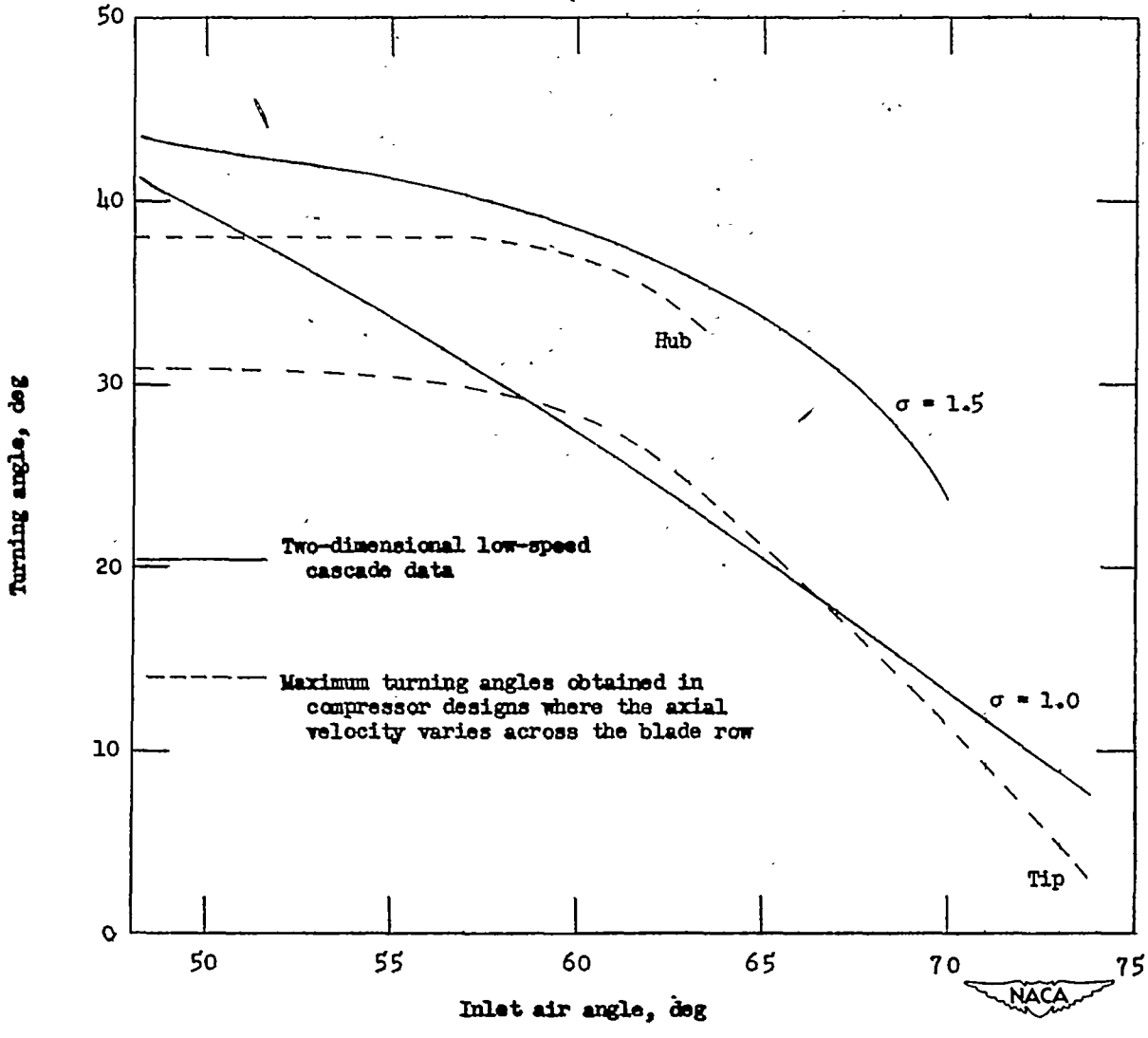

Figure 7.- Turning-angle limitations plotted against inlet air angle.

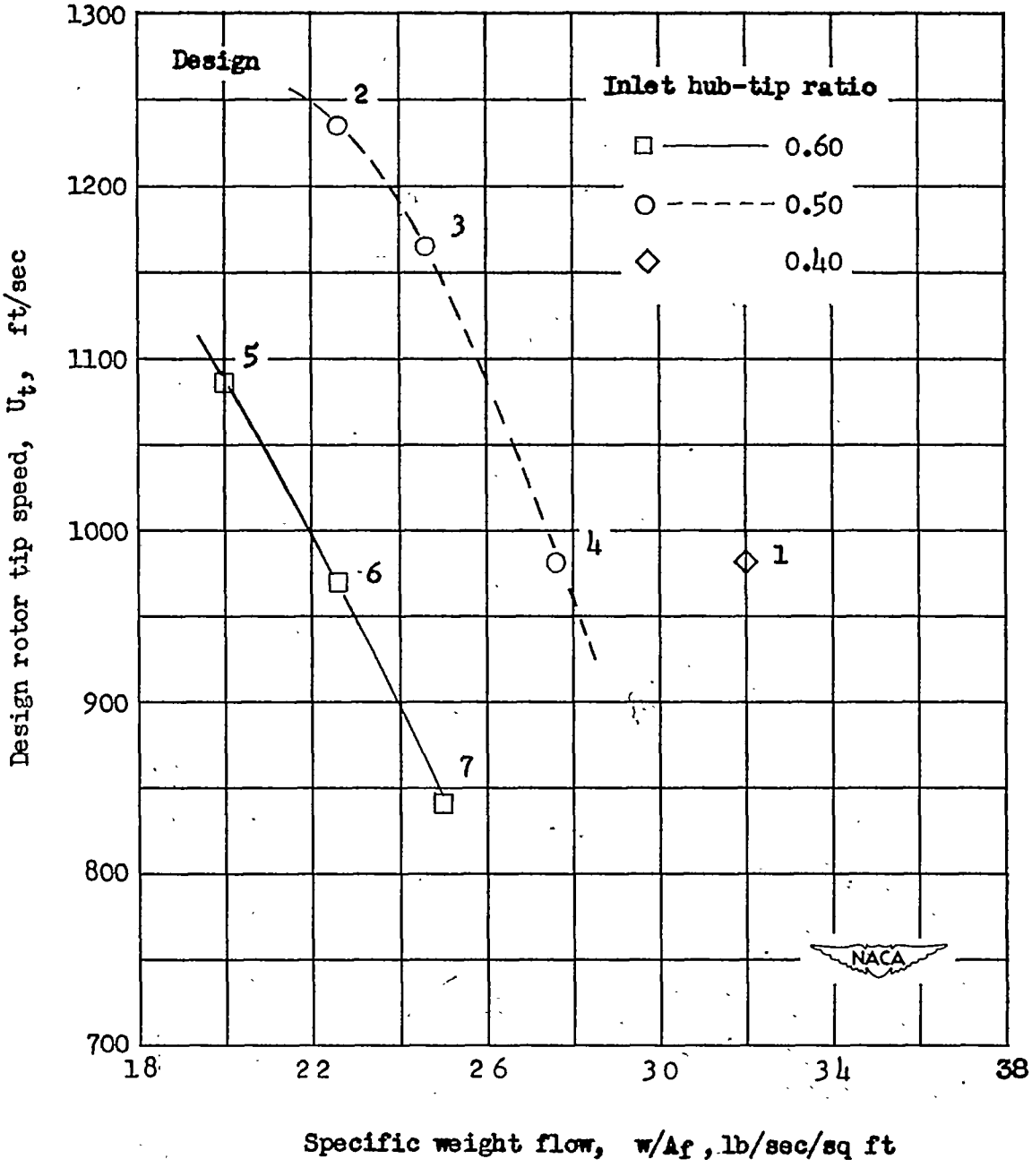

Figure 8.- Design rotor tip speed plotted against specific weight flow for inlet hub-tip ratios of 0.40, 0.50, and 0.60.

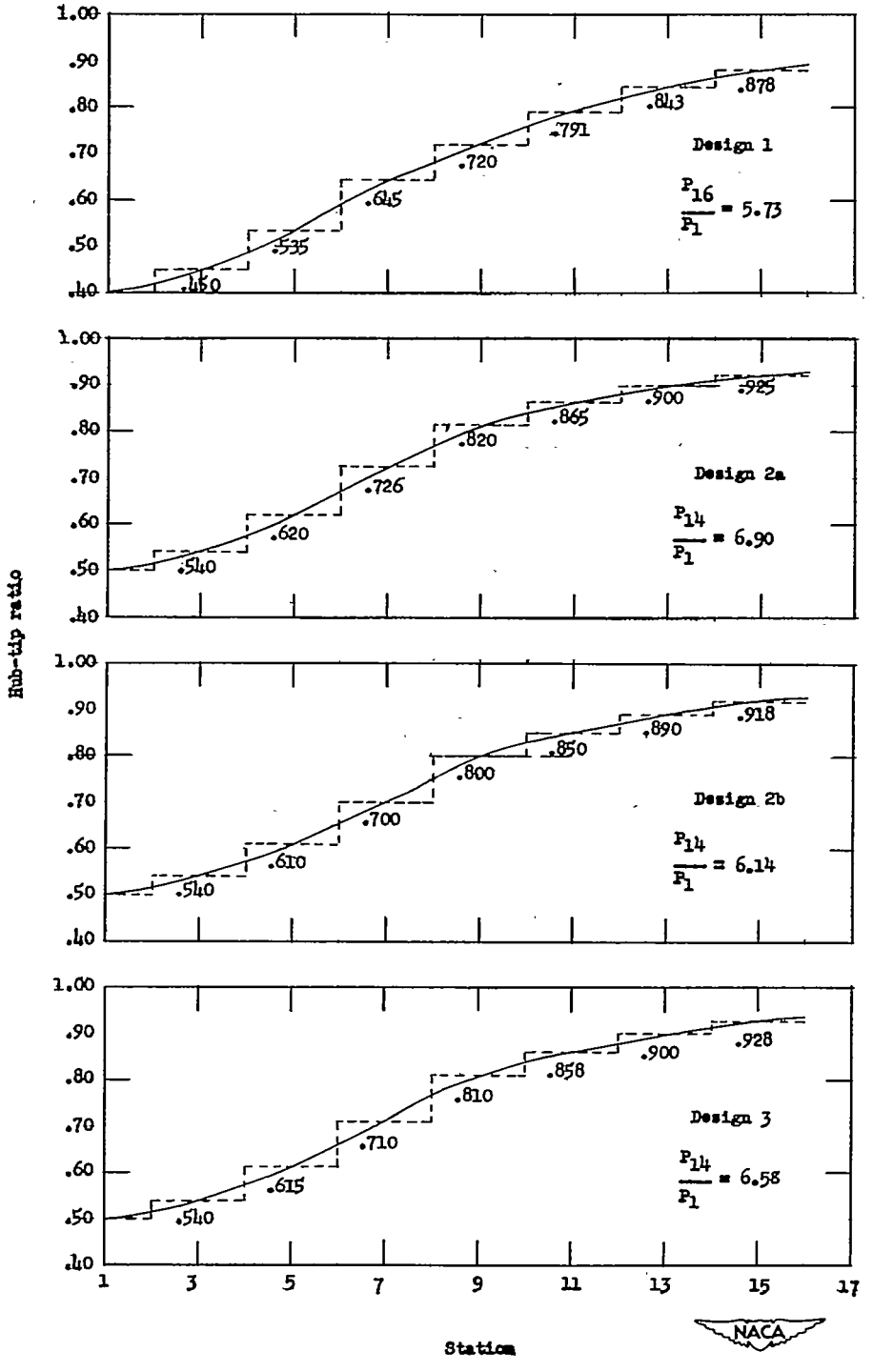

(a) Designs 1 to 3.

Figure 9.- Hub contour plotted against station. Dashed lines and values indicate the hub-tip ratios used in the untapered stage calculations to approximate the actual tapered stages.

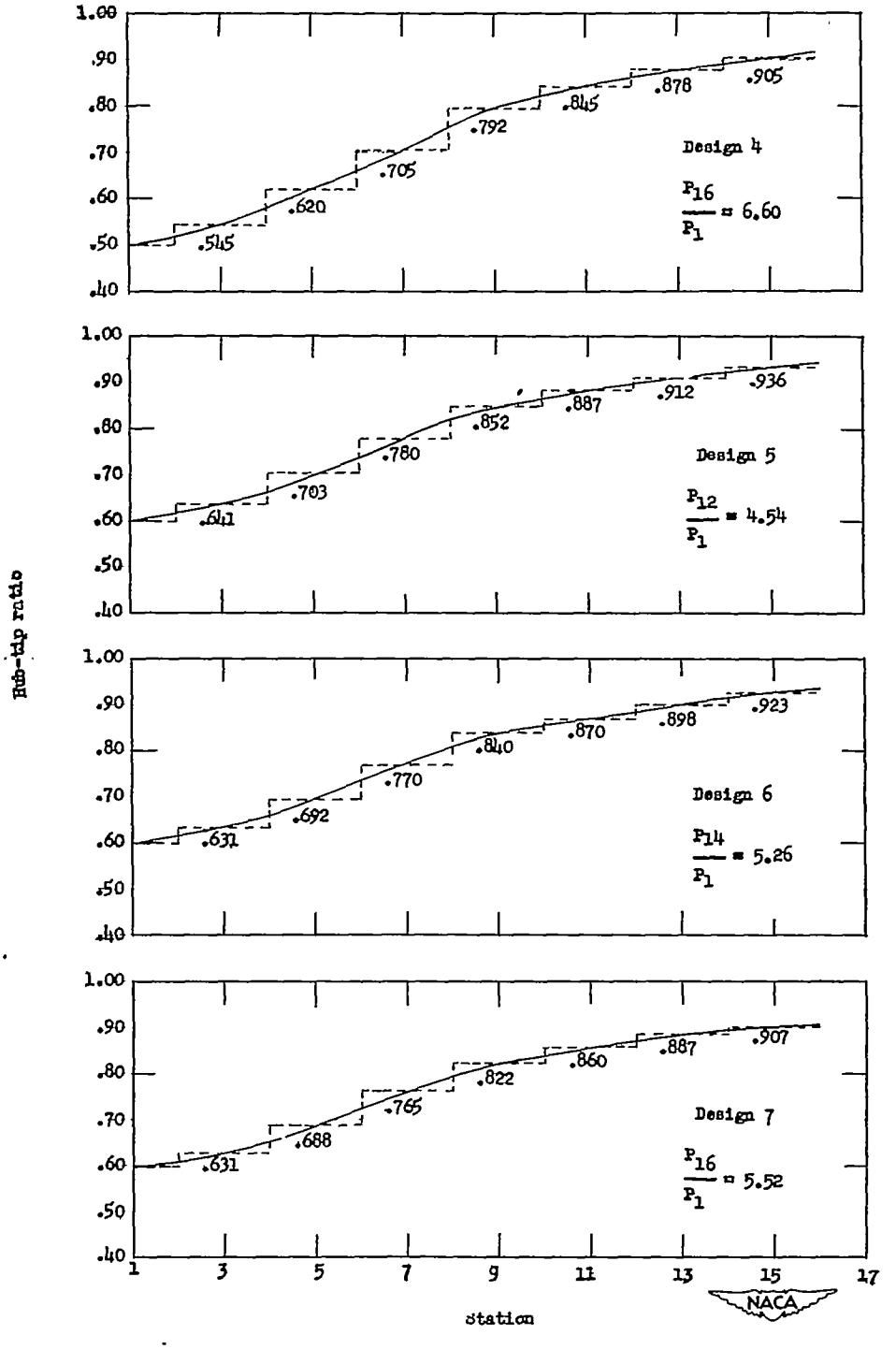

(b) Designs 4 to 7.

Figure 9.- Concluded.

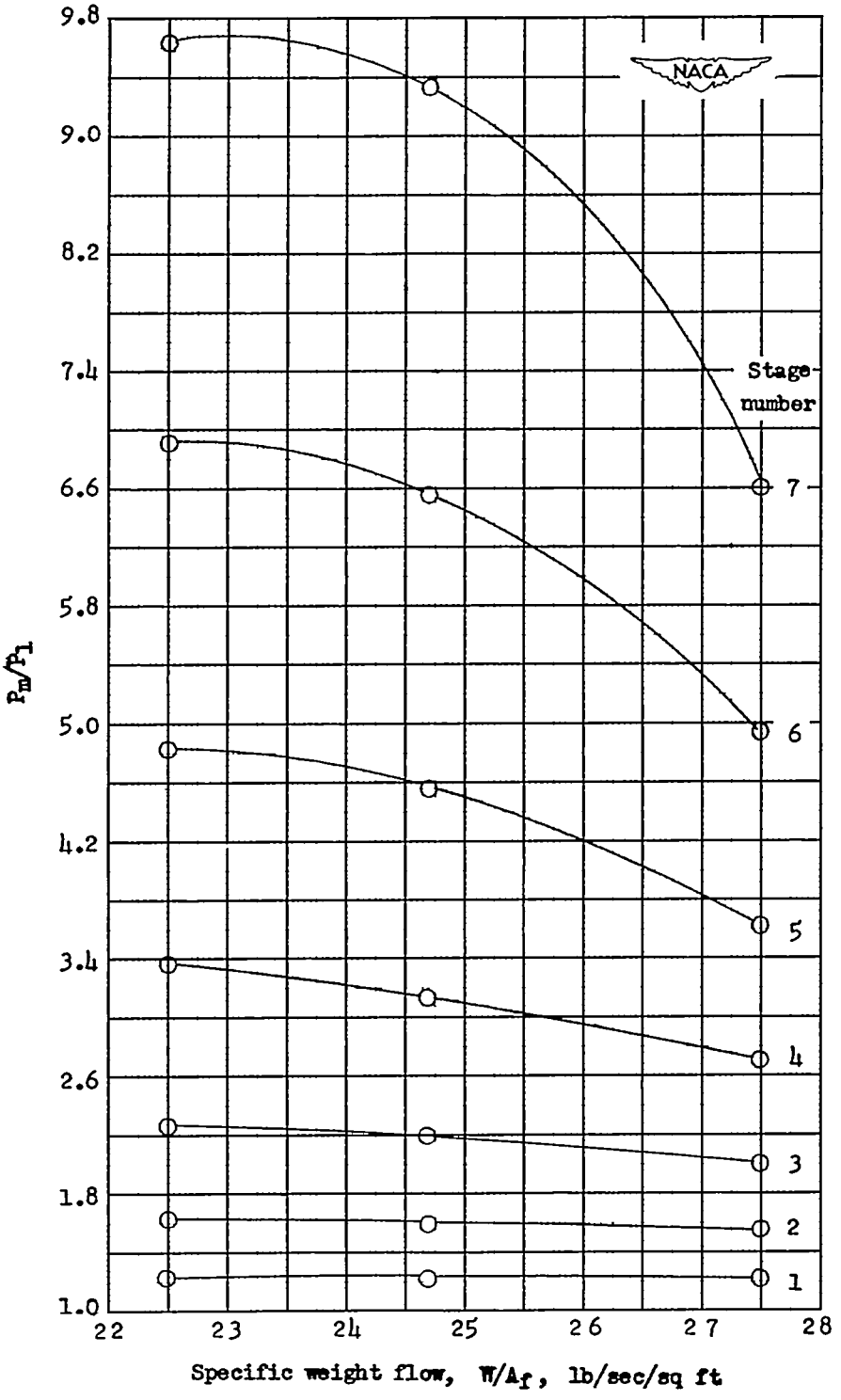

Figure 10.- Ratio of total pressure at mean-radius section of the succeeding stages to inlet total pressure plotted against specific weight flow at an inlet hub-tip ratio of 0.50.

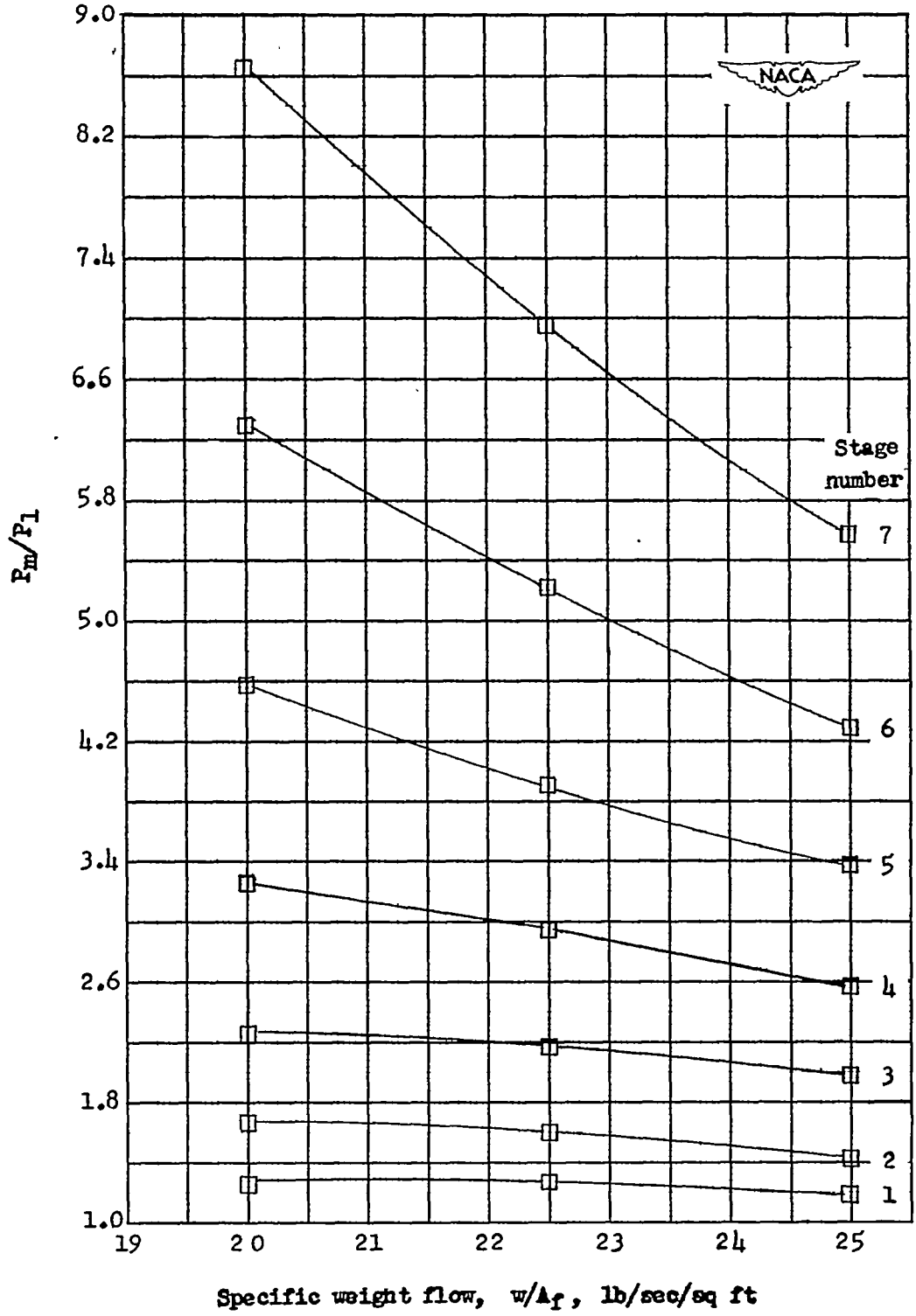

Figure 11.- Ratio of total pressure at mean-radius section of the succeeding stages to inlet total pressure plotted against specific weight flow at an inlet hub-tip ratio of 0.60.

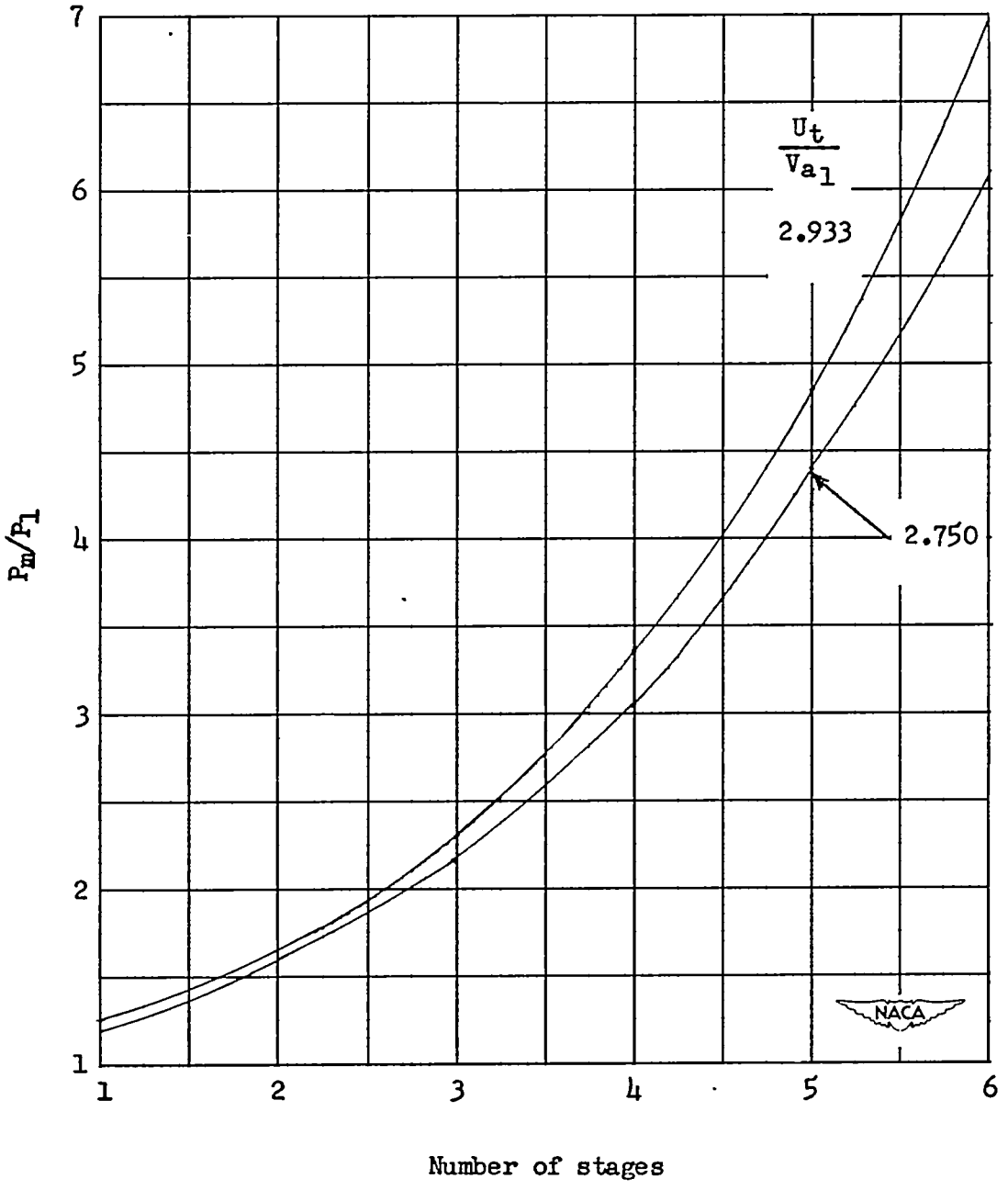

Figure 12.- Ratio of total pressure at mean-radius section to inlet total pressure plotted against number of stages for U_t/V_{a_1} of 2.933 (design 2a) and 2.750 (design 2b) at a specific weight flow of 22.5 pounds per second per square foot frontal area.

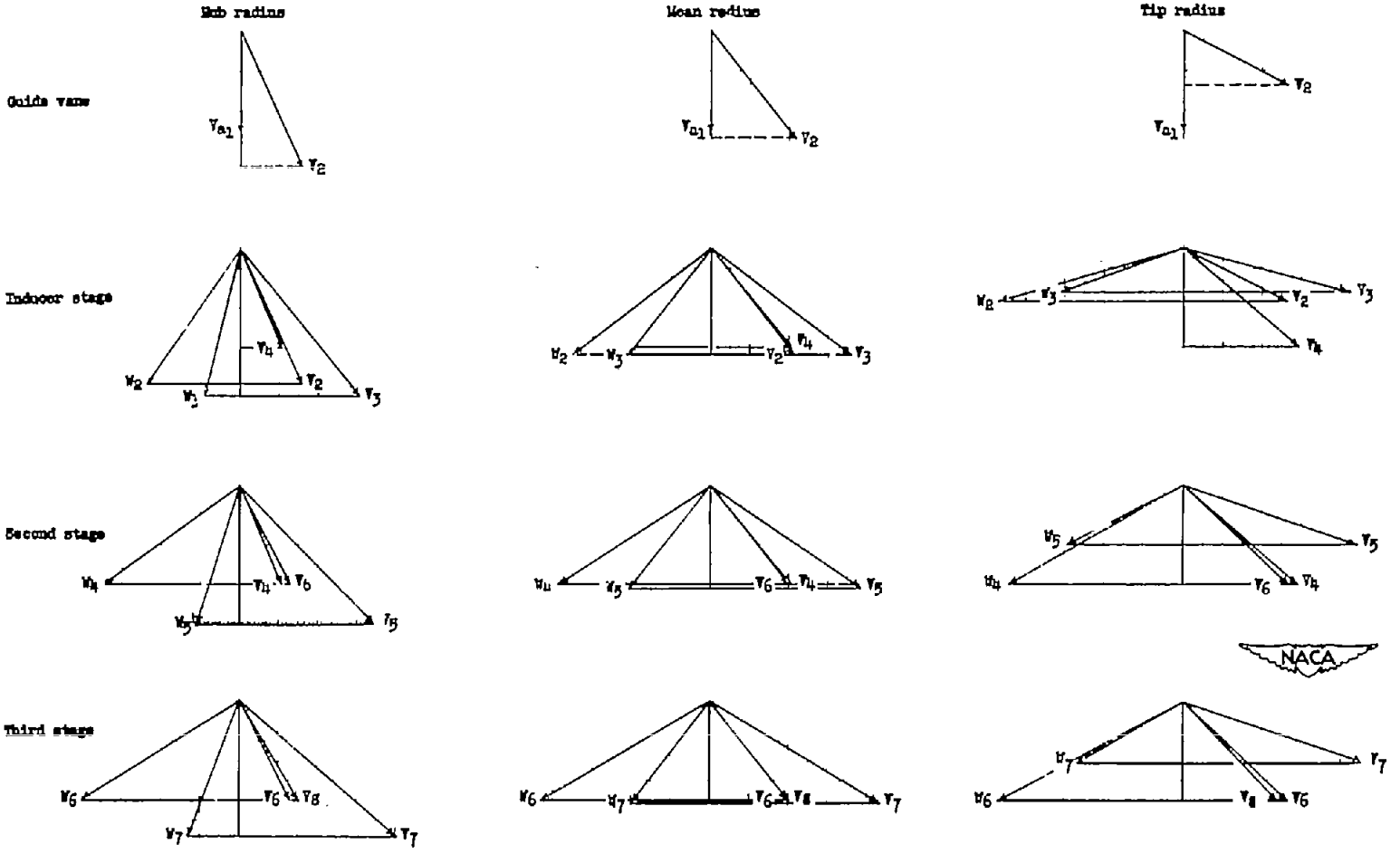

(a) Stages 1 to 3.

Figure 13.- Velocity diagrams at hub, mean radius, and tip for design 2a. $\frac{W}{A_f}$ = 22.5 pounds per second per square foot; $\frac{U_t}{V_{a_1}}$ = 2.933; $\frac{r_h}{r_t}$ = 0.50.

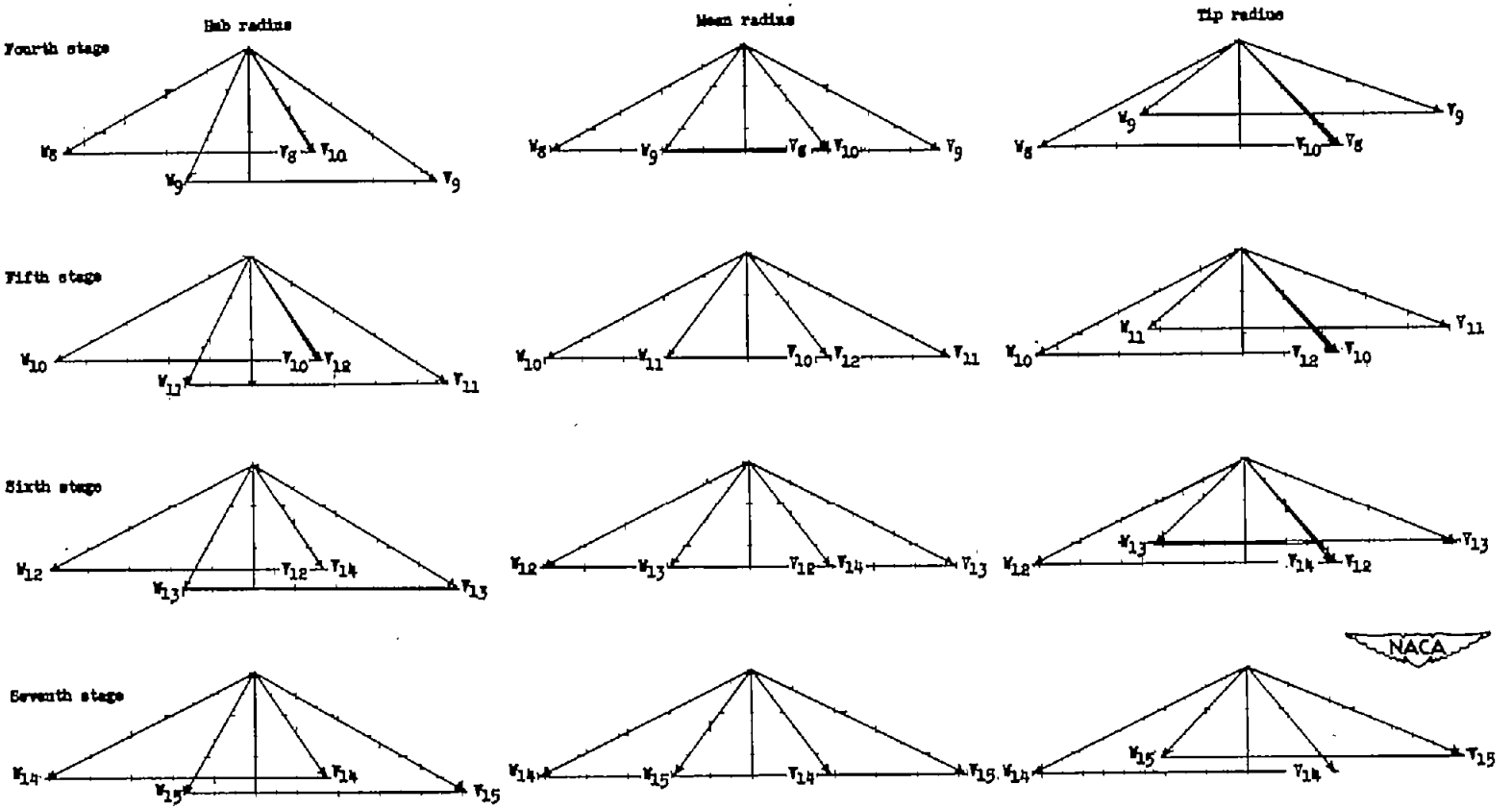

(b) Stages 4 to 7.

Figure 13.- Concluded.

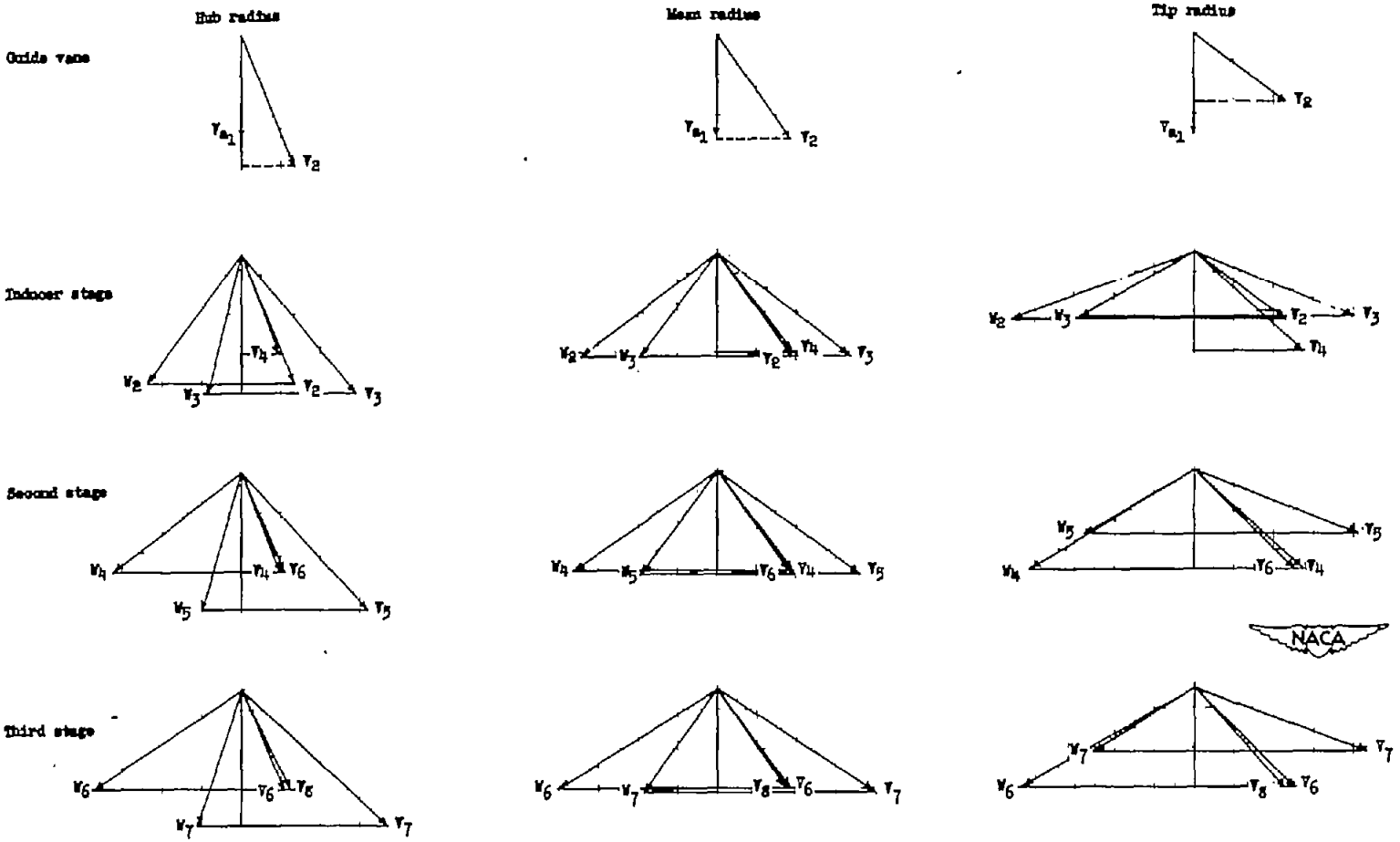

(a) Stages 1 to 3.

Figure 14.- Velocity diagrams at hub, mean radius, and tip for design 2b. $\frac{W}{A_f}$ = 22.5 pounds per second per square foot; $\frac{U_t}{Va_1}$ = 2.750; $\frac{r_h}{r_t}$ = 0.50.

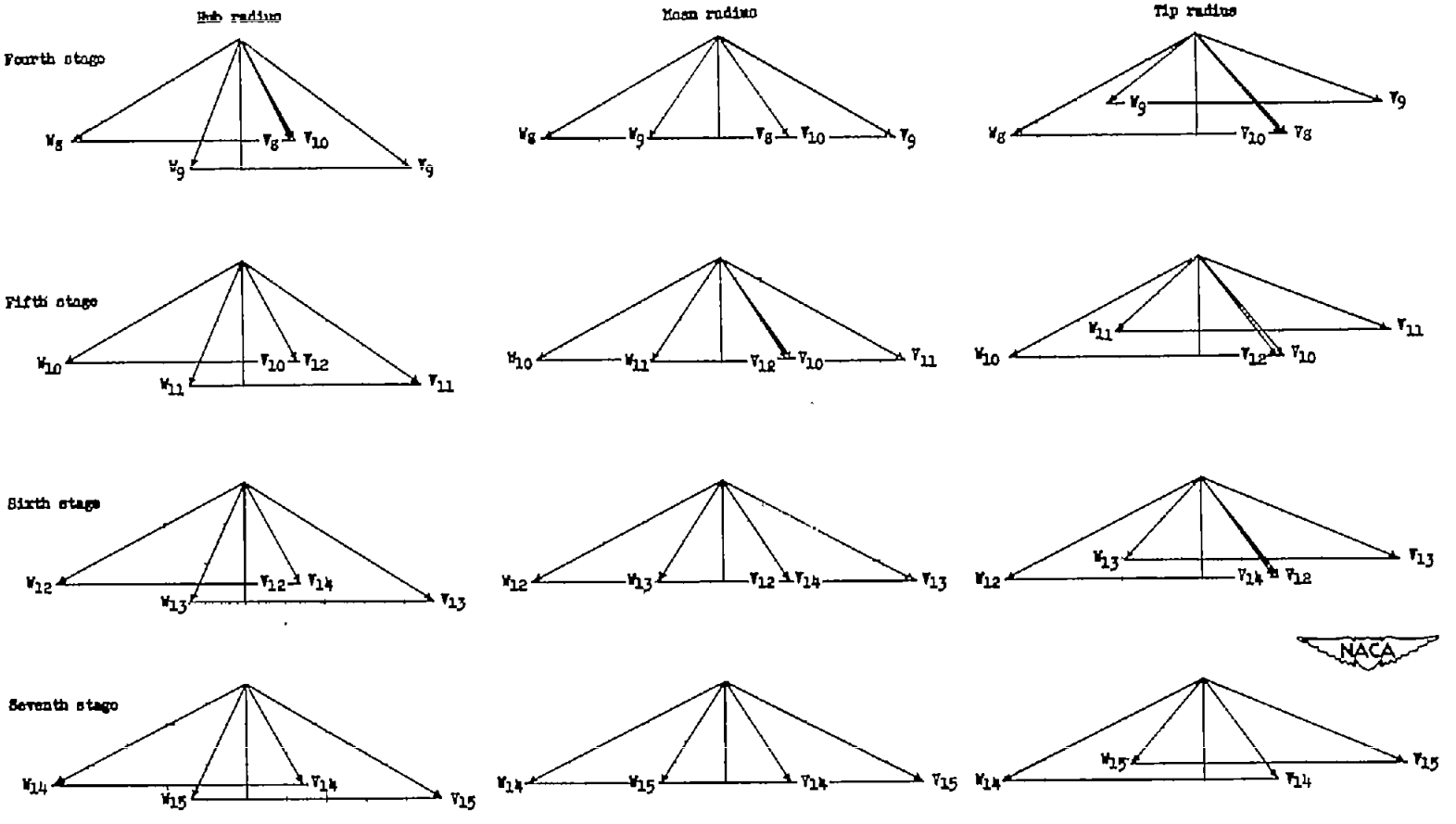

(b) Stages 4 to 7.

Figure 14.- Concluded.

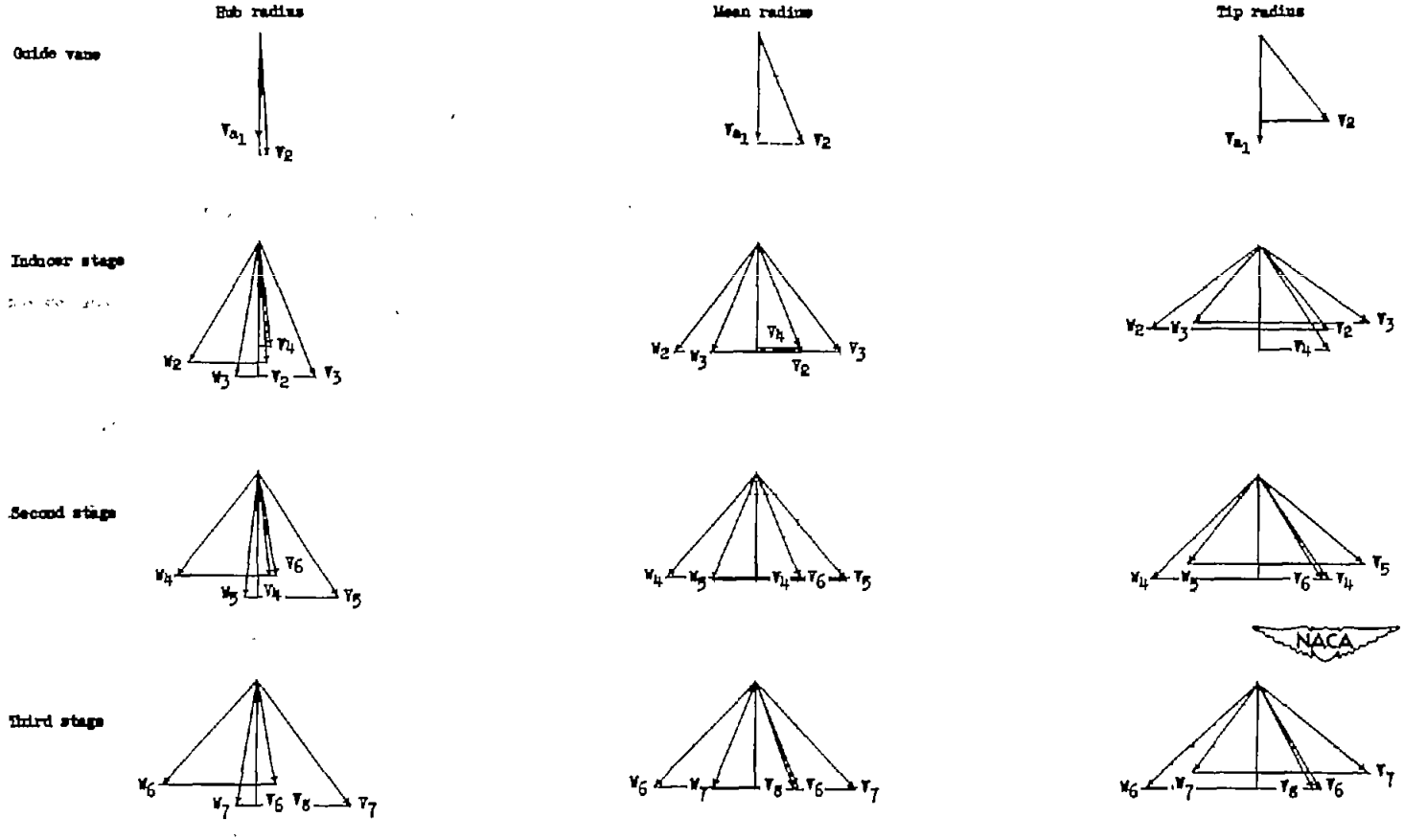

(a) Stages 1 to 3.

Figure 15.- Velocity diagrams at hub, mean radius, and tip for design 1. $\frac{W}{A_f}$ = 32.5 pounds per second per square foot; $\frac{U_t}{V_{a_1}}$ = 1.684; $\frac{r_h}{r_t}$ = 0.40.

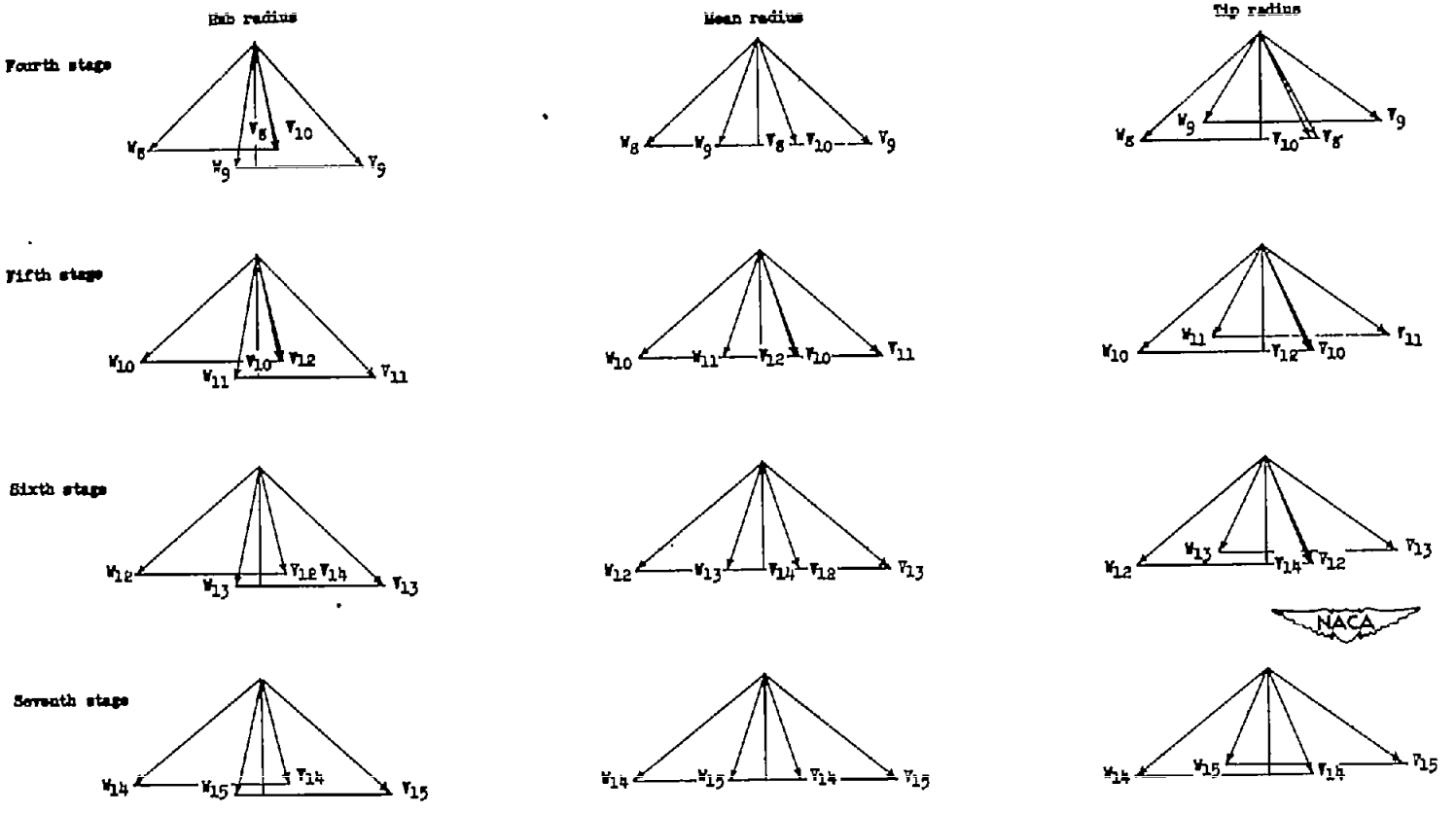

(b) Stages 4 to 7.

Figure 15.- Concluded.

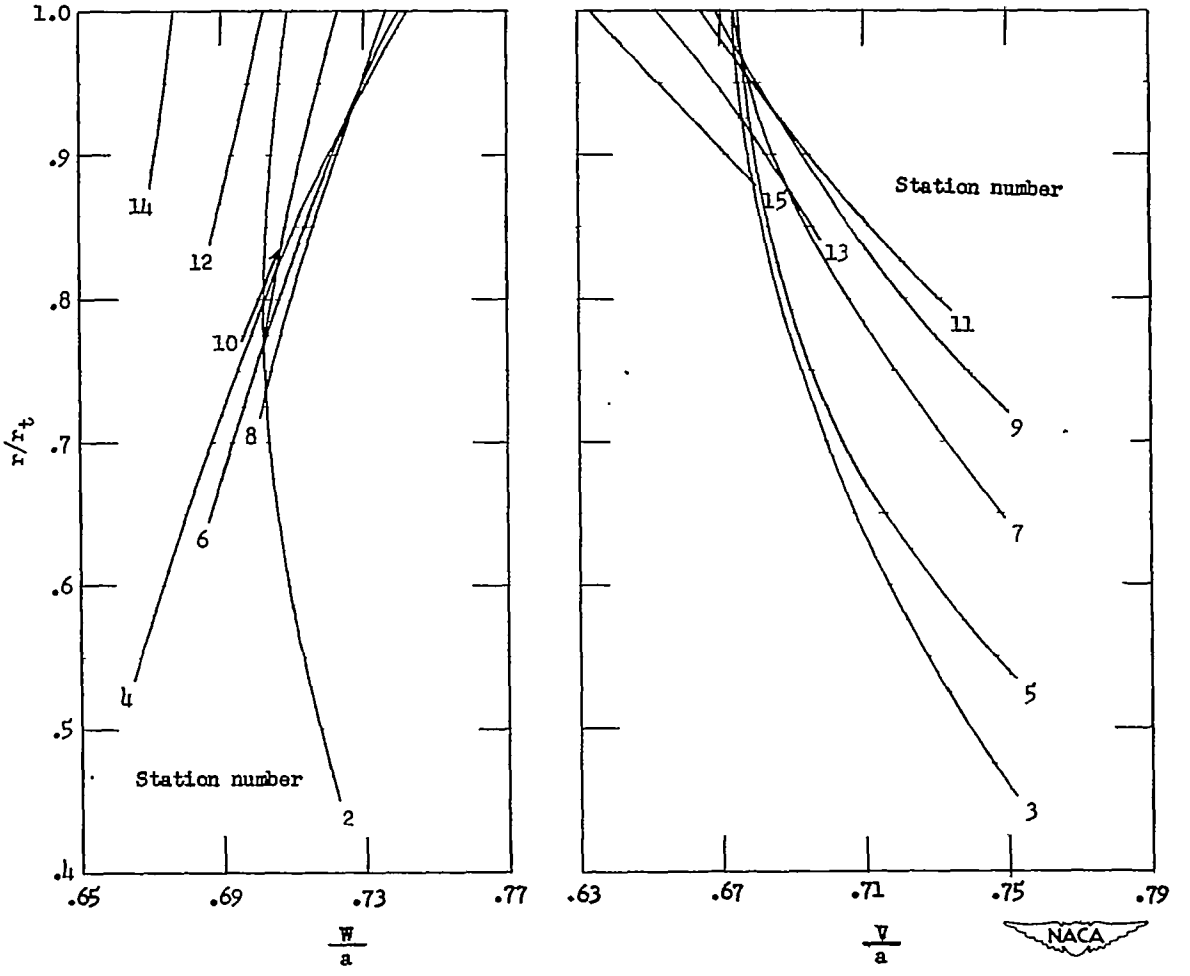

(a) Relative inlet Mach numbers at stations 2 to 15.

Figure 16.- Flow conditions through a typical multistage compressor with inlet hub-tip ratio of 0.40 and specific weight flow of 32.5 pounds per second per square foot of frontal area. (Design 1.)

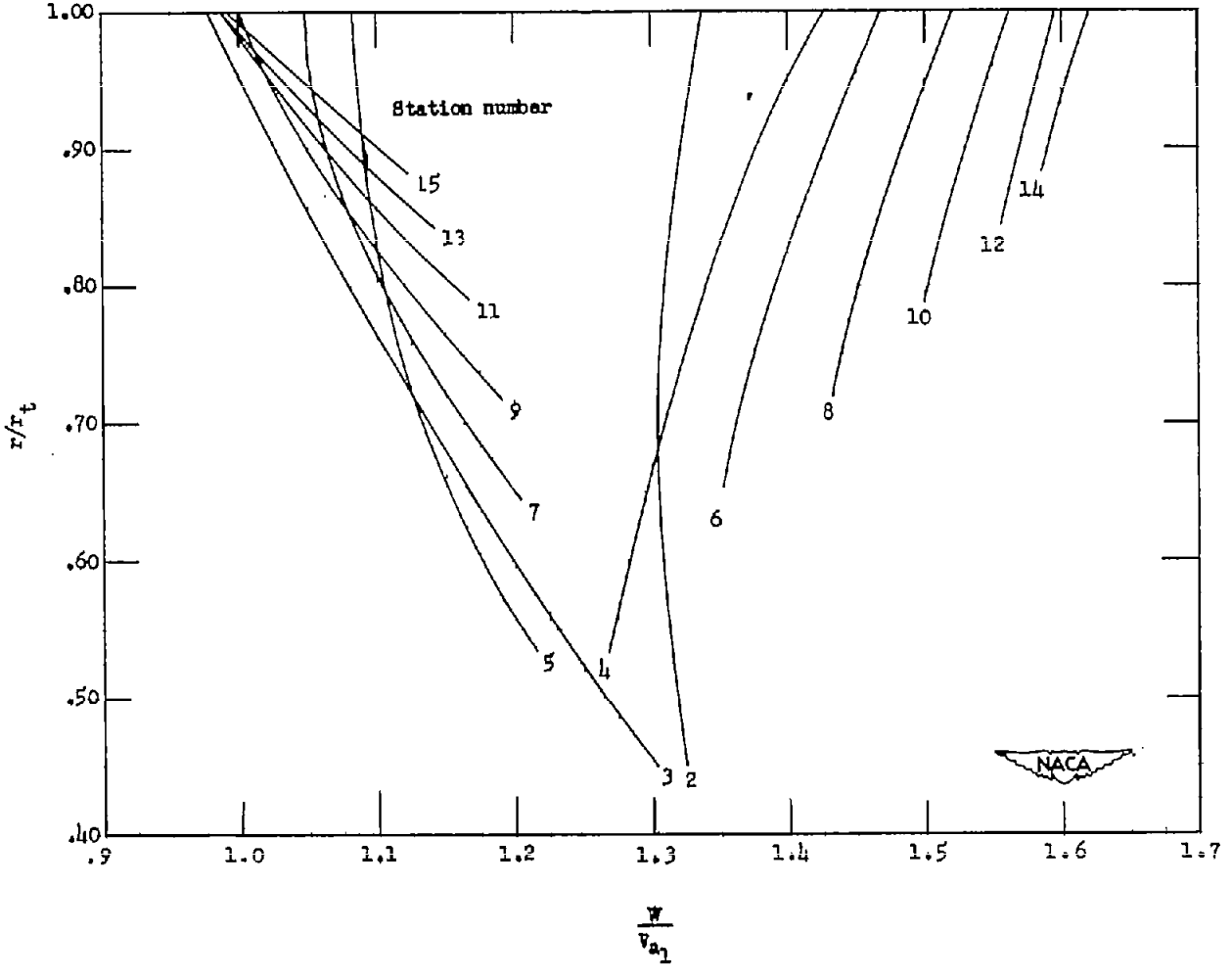

(b) Ratios of velocity relative to rotor to inlet axial velocity at stations 2 to 15.

Figure 16.- Continued.

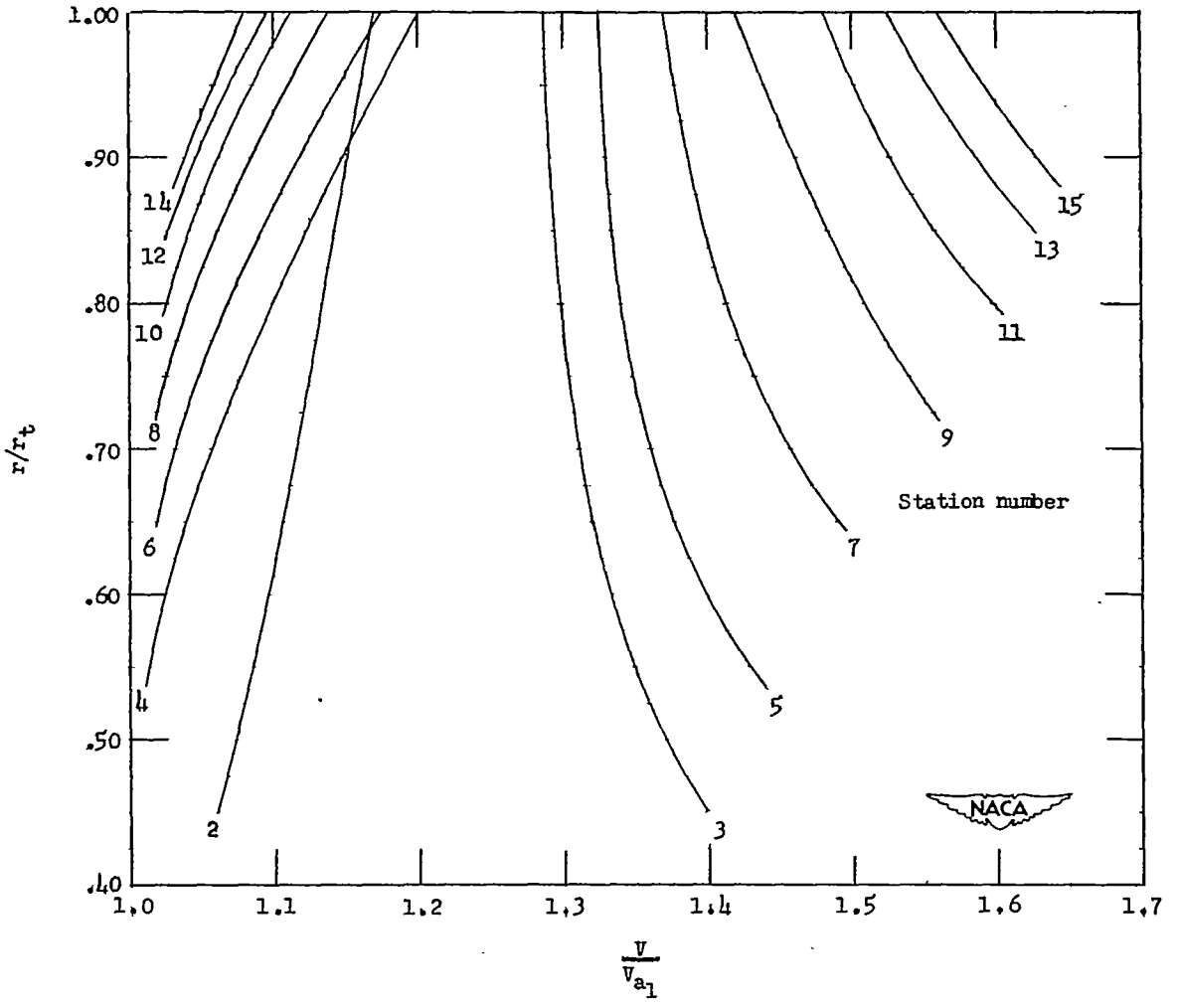

(c) Ratios of velocity relative to stator to inlet axial velocity at stations 2 to 5.

Figure 16.- Continued.

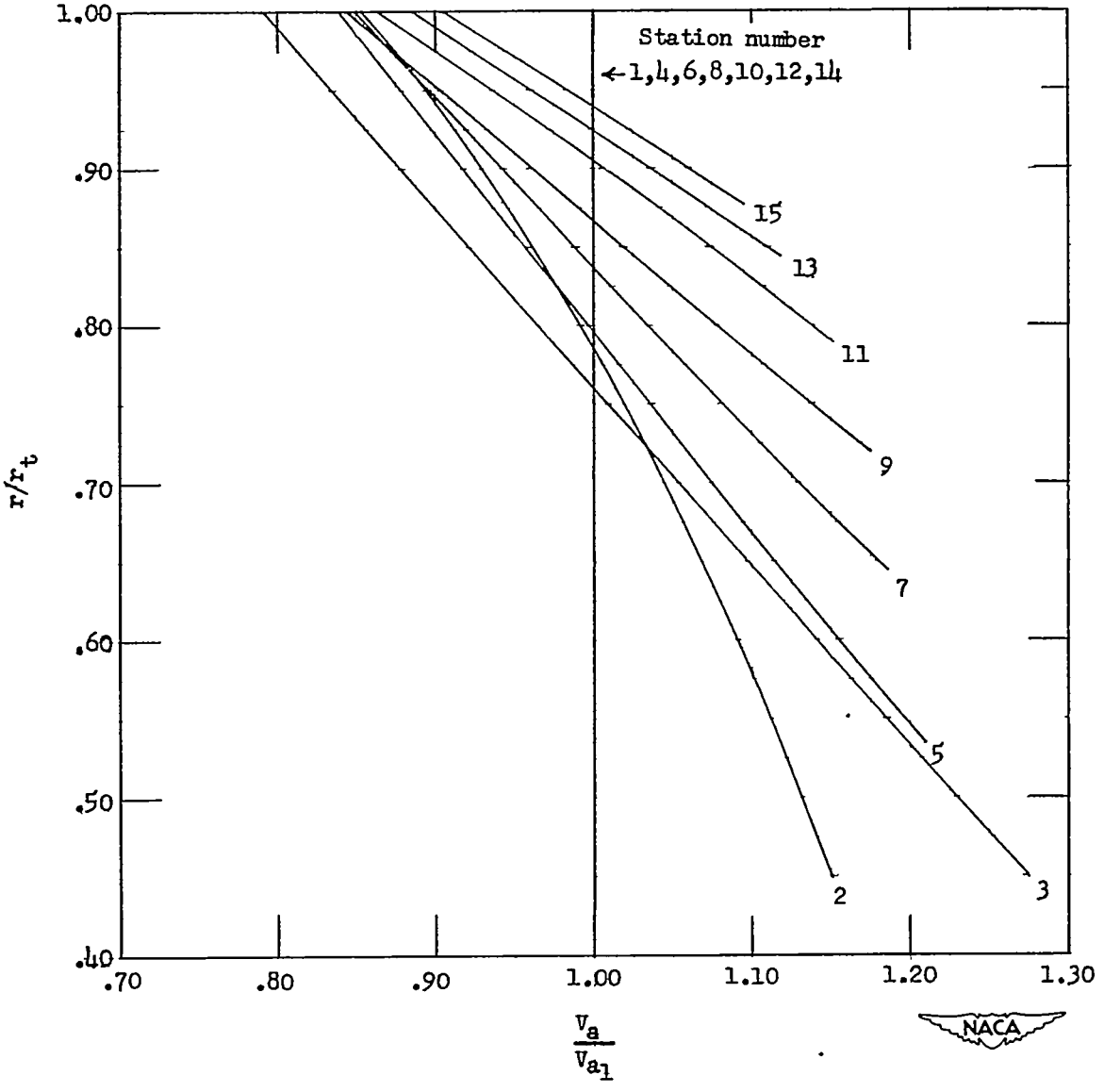

(d) Ratio of axial velocity to inlet axial velocity at stations 1 to 15.

Figure 16.- Continued.

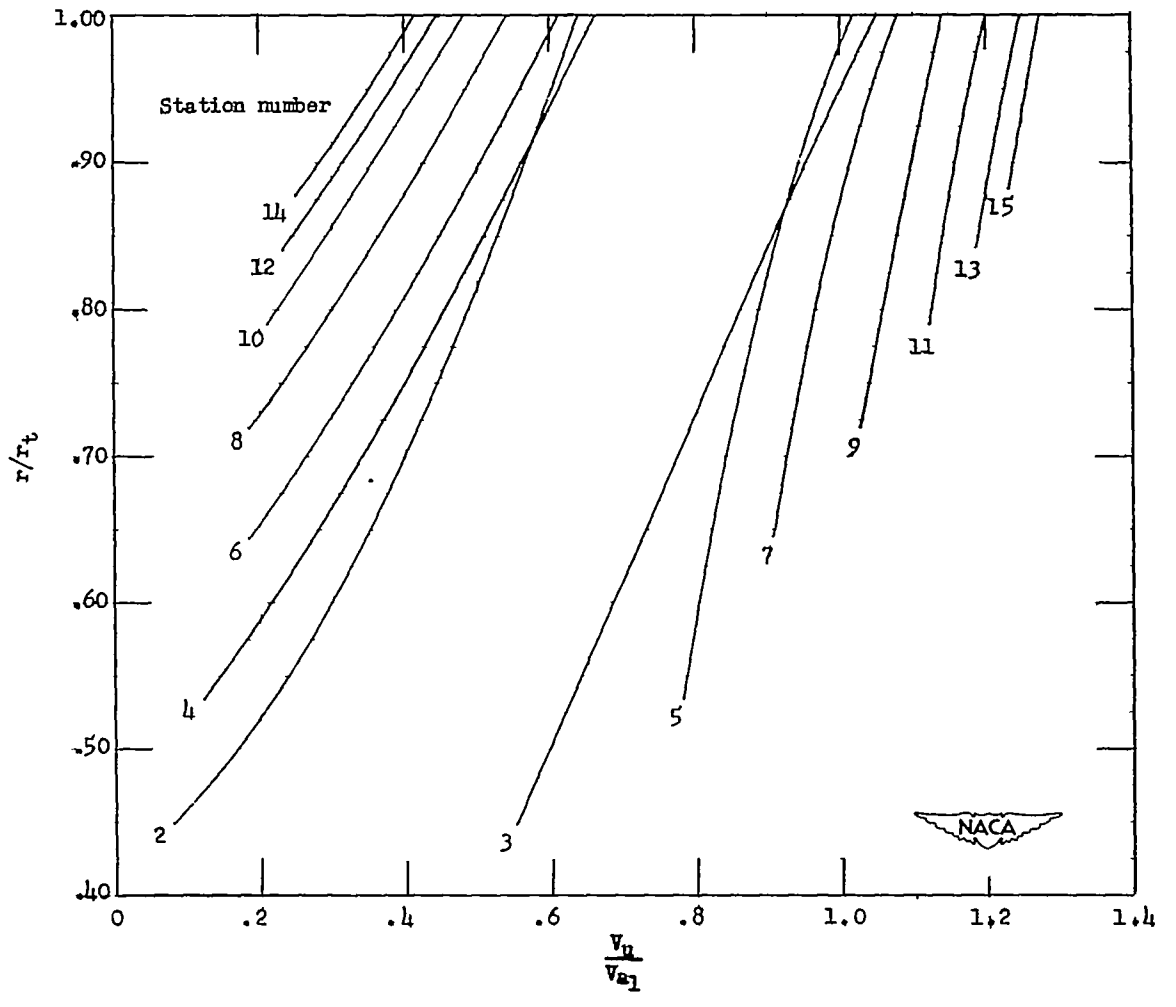

(e) Ratio of tangential velocity to inlet axial velocity at stations 2 to 15.

Figure 16.- Continued.

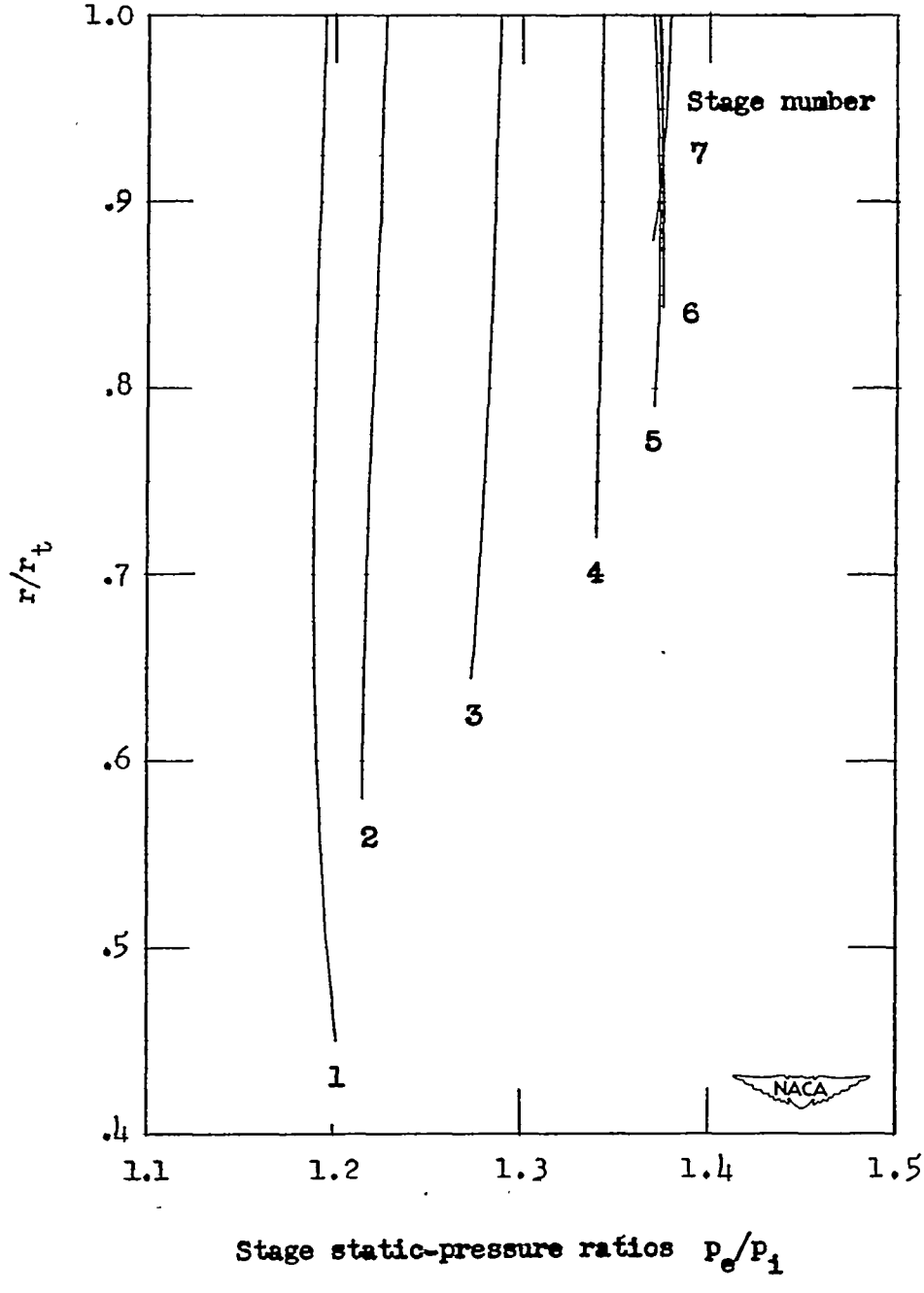

(f) Static-pressure ratios across each stage.

Figure 16.- Concluded.

NACA-Langley - 3-12-52 - 1000